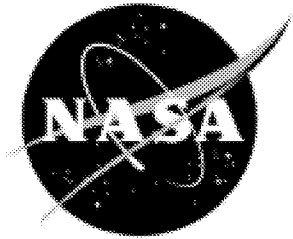NASA/TM-2002-211781

Prediction of Long-Term Strength of Thermoplastic Composites Using Time-Temperature Superposition

James R. Reeder
Langley Research Center, Hampton, Virginia

August 2002

The NASA STI Program Office . . . in Profile

Since its founding, NASA has been dedicated to the advancement of aeronautics and space science. The NASA Scientific and Technical Information (STI) Program Office plays a key part in helping NASA maintain this important role.

The NASA STI Program Office is operated by Langley Research Center, the lead center for NASA's scientific and technical information. The NASA STI Program Office provides access to the NASA STI Database, the largest collection of aeronautical and space science STI in the world. The Program Office is also NASA's institutional mechanism for disseminating the results of its research and development activities. These results are published by NASA in the NASA STI Report Series, which includes the following report types:

- TECHNICAL PUBLICATION. Reports of completed research or a major significant phase of research that present the results of NASA programs and include extensive data or theoretical analysis. Includes compilations of significant scientific and technical data and information deemed to be of continuing reference value. NASA counterpart of peer-reviewed formal professional papers, but having less stringent limitations on manuscript length and extent of graphic presentations.

- TECHNICAL MEMORANDUM. Scientific and technical findings that are preliminary or of specialized interest, e.g., quick release reports, working papers, and bibliographies that contain minimal annotation. Does not contain extensive analysis.

- CONTRACTOR REPORT. Scientific and technical findings by NASA-sponsored contractors and grantees.

- CONFERENCE PUBLICATION. Collected papers from scientific and technical conferences, symposia, seminars, or other meetings sponsored or co-sponsored by NASA.

- SPECIAL PUBLICATION. Scientific, technical, or historical information from NASA programs, projects, and missions, often concerned with subjects having substantial public interest.

TECHNICAL TRANSLATION. English-language translations of foreign scientific and technical material pertinent to NASA's mission.

Specialized services that complement the STI Program Office's diverse offerings include creating custom thesauri, building customized databases, organizing and publishing research results . . . even providing videos.

For more information about the NASA STI Program Office, see the following:

- Access the NASA STI Program Home Page at *http://www.sti.nasa.gov*

- Email your question via the Internet to help@sti.nasa.gov

- Fax your question to the NASA STI Help Desk at (301) 621-0134

- Telephone the NASA STI Help Desk at (301) 621-0390

- Write to:
  NASA STI Help Desk
  NASA Center for AeroSpace Information
  7121 Standard Drive
  Hanover, MD 21076-1320

NASA/TM-2002-211781

Prediction of Long-Term Strength of Thermoplastic Composites Using Time-Temperature Superposition

James R. Reeder
Langley Research Center, Hampton, Virginia

August 2002

ABSTRACT

The compliance and strength of polymeric composite materials may change over time in high temperature or long service applications. To avoid failures due to unexpected strength loss after long periods of time, it is imperative that accelerated tests be developed to determine long-term strength properties. Constant ramp transverse strength tests on thermoplastic composite specimens were conducted at four temperatures from 300°F to 450°F and five duration times from 0.5 sec to 24 hrs. Up to 400°F, the time-temperature-superposition method produces a master curve allowing strength at longer times to be estimated from strength tests conducted over shorter times but at higher temperatures. The shift factors derived from compliance tests applied well to the strength data. To explain why strength behaved similar to compliance, a viscoelastic fracture model was investigated based on the hypothesis that the work of fracture for crack initiation at some critical flaw remains constant with time and temperature. The model, which used compliance as input, was found to fit the strength data only if the critical fracture energy was allowed to vary with stress rate. Fracture tests using double cantilever beam specimens were conducted from 300°F to 450°F over time scales similar to the strength study. The toughness data showed a significant change with loading rate, less variation with temperature, did not form a master curve, and could not be correlated with the fracture model. Since the fracture model did not fit the fracture data, an alternative explanation based on the dilatational strain energy density was proposed. This model produced the same predictions for transverse strength as the fracture model. The dependence of the critical parameter on loading rate severely limits the use of these criteria for developing accelerated tests.

This research showed that strength does form a master curve using compliance shift factors from 300°F to 400°F (but not at 450°F) and showed that both strength and toughness changed significantly with time. The significance of this research is therefore seen as providing both the hope that a more versatile acceleration method for strength can be developed and the proof that such a test is needed.

ACKNOWLEDGMENTS

This paper covers the research conducted in fulfillment of the research requirement for a Ph.D. degree in Mechanical Engineering from Texas A&M University. The author would like to thank his committee co-chairs, Walter L. Bradley and David H. Allen, as well as the rest of his graduate committee, H. J. Sue, J. N. Reddy, and Charles E. Harris.

The author wishes to thank the National Aeronautics and Space Administration for the opportunity to complete the requirements for this degree and to I. S. Raju, the Head of the Mechanics of Materials Branch at NASA Langley Research Center for his support and encouragement during this research project. The author would also like to thank his coworkers within the Mechanics of Materials Branch for the technical discussions that have sparked his understanding and interest within the research area, and in particular, he would like to thank the three individuals who have acted as mentors through the years: Dr. John Crews, Jr., Dr. Kevin O'Brien, and Dr. Charles Harris.

The author is grateful to Dr. Walter L. Bradley and Dr. David H. Allen for their guidance and support during the last several years and especially for their help in overcoming the special problems associated with finishing up an advanced degree from out of state.

Finally the author would like to thank the friends and family who have supported him through these years of study with care and understanding. Special thanks are extended to Willa Mae and Charles, the author's mother and father, for instilling since childhood their belief in the importance of education.

TABLE OF CONTENTS

LIST OF FIGURES

NOMENCLATURE

a	Delamination crack length, in.
Δa	Delamination extension, in.
A	Material constant
A_T	Shift factor
b	Thickness, in.
c	Dimension of micromechanics model, in.
C	Constant
D	Compliance, in^2/lb
DCB	Double cantilever beam test
E	Elastic modulus, psi
$\mathcal{E}_{dil}$	Dilatational strain energy density, $in\text{-}lb/in^3$
ERR	Energy release rate, $in\text{-}lb/in^2$
F	Function of time for strain and displacement in correspondence problems
f	Functional relationship
G	Toughness, $in\text{-}lb/in^2$
H	Function of time for stress in correspondence problems
ΔH	Activation energy, $in\text{-}lb/mole$
J	J integral fracture parameter, , $in\text{-}lb/in^2$
m	Slope of loading curve, in/lb
P	Applied load, lbs
r	Process rate, $1/sec$
R	Rate of loading, lb/sec

R	Ideal gas constant, in-lb/mole-°R
t	Time, sec
T	Temperature, °F
T_R	Temperature, °R
u	Displacement in the x direction, in.
U	Strain energy, in-lb
U	Uniform displacement value in the x direction, in.
v	Displacement in the y direction, in.
V	Uniform displacement value in the y direction, in.
w	Width, in.
W_f	Work of fracture, in-lb/in^2
α	Shift rate
β	Constant in stretched exponential equation
δ	Load-point displacement, in.
δ_{CTOD}	Critical displacement at the crack tip
ε	Strain, in/in
η	Time-temperature shift rate, °R
μ	Aging shift rate, psi
σ	Stress, psi
τ	Material time constant, sec.
υ	Volume fraction
ν	Poisson's ratio
ψ	Dummy time variable, sec

Subscripts

1,2	Denotes distinct values
Ic	Indicates mode I toughness
age	Pertaining to the aging period
c	Pertaining to the composite
crit	Pertaining to the critical value
f	Pertaining to the fiber
F	Pertaining to the flow stress
g	Pertaining to the glass transition point
i	Denotes crack initiation value
m	Pertaining to matrix
max	Pertaining to the maximum load point on loading curve
nl	Pertaining to the point of nonlinearity on loading curve
o	Denotes initial value
ref	Pertaining to the reference value
v	As calculated from the reference elastic problem
xx, xy, yy, zz	Denotes tensorial values

Superscripts

E	Pertaining the reference elastic problem
max	Pertaining to the maximum value

CHAPTER I

INTRODUCTION

The next generation of supersonic aircraft will fly at speeds that will cause significant heating of the aircraft structure due to friction with the atmosphere. Some estimates put the structural service temperature of such an aircraft at 375°F [1]. This temperature is far beyond the service temperature of normal composite resins such as epoxies that often cure at 375°F. Advanced resins are therefore being developed that possess long-term structural integrity at these elevated service temperatures. As the service temperature is pushed higher and higher, the selection of materials and the determination of design strain allowables must be established so that time-dependent behavior is fully taken into account. One concern is that, during a service life of 20 years at elevated temperature, the time-dependent response of the resin may allow damage to initiate and grow. This damage would not be predicted from normal short term laboratory tests. Since real time tests lasting 20 years are impractical, accelerated tests must be developed to simulate the damage that might occur over long periods of time.

The eventual goal is to develop models that are able to predict damage that will initiate and grow in structures that are in service for decades. These models will have to be able to model full thermo-mechanical fatigue accounting for viscoelastic deformation, plastic deformation, physical and chemical aging, and environmental effects. One step toward the final goal would be to accurately predict the long-term static strength of composite materials using much shorter-term strength tests. The development of such an accelerated test for strength is the objective of this dissertation project.

Objective and Scope

The literature review (presented in Chapter II of this dissertation) suggests that it may be possible to accelerate the strength testing of advanced composite materials by elevating the test temperature as is commonly done for compliance properties. It is the objective of this research program to first demonstrate that the strength properties of the thermoplastic class of composite material are significantly effected by time. The second objective is to determine whether temperature can be used as an accelerator for strength. For temperature to be used as an accelerator, it must change the strength properties in a controlled manner so that an elevation in temperature produces a similar effect as a known shift in the time scale. This means that the strength data at different temperatures can be shifted in time to form a master curve. It has been suggested in the literature that the same constant used for the modulus data can be used to form strength master curves. If so, the third objective will be to explain why the time-temperature relationship of strength and modulus are tied together in this way.

The experimental research program will include two parts. In the first part, transverse tension strengths of a IM7/K3B composite will be tested over a wide range of time scales and at several temperatures. At each temperature, the strength will be determined as a function of loading rate to show the magnitude of the time scale effect. Once the failure curves are defined at different temperatures, they can be shifted to see if they will form a master curve. The shift factors can then be compared to see if they are the same as the shift factors used for modulus data.

The second part of the research program will focus on why the superposition of compliance and strength might be tied together. A viscoelastic fracture mechanics model will be presented which defines a critical fracture parameter based on viscoelastic compliance properties. The results of the fracture model will be compared to the strength

results. For the fracture model to be an appropriate model for these strength tests, the strength property must be controlled by a fracture type phenomenon where cracks initiate and grow from incipient flaws to cause failure. If this is the case, the strength results should behave similar to established fracture properties. A second study was conducted with the double cantilever beam (DCB) test for delamination toughness, which is an established fracture test. These tests were also performed over a wide range of time scales and at several temperatures. If the same phenomenon controls both types of tests, they should be effected similarly by time and temperature, thus indicating that a fracture model is an appropriate model for the strength tests. If the viscoelastic fracture model describes the DCB results as well as the transverse strength results, then the reason for time-temperature superposition working for "strength" will be largely explained due to the models dependence on modulus. A model of this type, which models failure based on compliance data, would not only make accelerated testing possible, but also dramatically reduce the number of strength tests needed to characterize a material's strength. Since strength testing is very expensive, this could result in a significant cost savings.

A second failure model based on the dilatational strain energy density will also be introduced as an alternative explanation to the fracture model. The predictions of the two failure models will be compared.

Following this brief introduction, this dissertation contains an extensive review of the relevant literature in Chapter II. Details of the materials used and the experimental procedures are presented in Chapter III. The analyses developed to understand the experimental results are presented in Chapter IV. In Chapter V, the results are presented along with discussion of these results. Finally, the conclusions from this investigation are presented in Chapter VI.

CHAPTER II

BACKGROUND

This chapter provides a background study of issues related to this research project. The first section describes the material and material modeling needs associated with building a high speed aircraft from polymeric composite materials. The next section reviews some computer tools available to help design laminated composite structures accounting for the effects of time. The phenomenon that can effect composite properties over time are reviewed next. These phenomenon are stress (fatigue damage), strain (viscoelasticity), chemical aging, and physical aging. The combined effects of these phenomenon are also reviewed. The next section reviews failure properties of composites. In this section only failure transverse to the fiber direction and composite toughness characteristics were covered. Methods of accelerating the effects of time on composites are reviewed in the next section. The last section provides a summary of the review.

Material Needs for Advanced High Speed Aircraft

In order to build the next generation of aircraft which is expected to fly at speeds between Mach 2 and 2.5 many key technical issues must be overcome. Cregger et al.[2] identified many key issues where advances must be made. In the category of materials, some of these key issues were long-term thermal aging, long-term creep, and thermomechanical fatigue. These are problems for the aircraft structural material because at Mach 2.4, the structure is expected to heat to temperatures of 310°F, and over the life time of the aircraft, the structure will be at temperature for 60,000 hours. The report pointed to the weight advantage of using polymeric composites for many parts often in a honeycomb type structures but noted the degradation expected for these materials at the high Mach numbers. Within these structures, it was reported that the polymer matrix

composites were primarily sized by strength and that improved damage tolerance criteria and degradation assumptions were needed.

A similar study by Brunner and Velicki[1] reported similar problems for the advanced aircraft. The peak temperature for the structure at Mach 2.4 was estimated at 375°F. Several critical technology development needs were listed such as improvements to polymeric composite stiffness while maintaining good operating strength, accelerated aging techniques and modeling to minimize expensive testing, and advanced materials development.

It is clear that, in order to build the structure of such a high speed aircraft, materials must be selected and designs must be made based an understanding of how well the material will perform for long periods of time under changing loads and environments. The environment conditions that the structural material will have to endure will most certainly include significant amounts of time at elevated temperature.

Design Programs

Polymeric composite materials were mentioned in the previous section as being an attractive option for the aircraft structure but problems with its degradation in properties were noted. There are a number of computer programs that attempt to model the properties and the degradation in properties, of composite materials subjected to various conditions. These programs use critical experimental data along with mathematical models to make their predictions.

MRLife[3] predicts the remaining strength of composite laminates subjected to fatigue loading. The computer code uses the strength and stiffness properties of the fiber and the matrix to compute laminae properties from various micromechanics models. The laminae properties are then used to predict laminate properties. Changes in constituent properties based on time (viscoelastic effects), physical aging and damage are predicted.

Matrix cracking, delamination growth, fiber buckling and fiber crushing are among the different damage mechanisms modeled.

ISAAC[4] (Integrated Strength Analysis for Aged Composites) is another computer code that attempts to model the tension and compression strength of laminates. This code incorporates models that account for such phenomenon as the oxidation of the matrix and physical aging effects on both notched and un-notched strength. A Tsai-Hill laminae failure criteria is used to predict failure in each ply leading to final failure of the 0° plies. The effect of matrix cracking and delamination are also included.

DAMLAM [5] uses a meso-scaled composite damage model (MCDM) to predict laminate stiffness and strength[6]. Within this model damage is assumed to be uniform throughout the thickness of an individual laminae. Damage growth under tension and compression stresses both static and cyclic are predicted. Inelastic strain and various damage mechanism are accounted for by the model.

These are only a few of the laminate property prediction codes available, with each having its own unique capabilities. To design the aircraft structure of a high speed aircraft, the capability of predicting strength and stiffness after extremely long periods of time at elevated temperature will be needed. The predictions of the computer code can only be as good as the models that the programs rely on and the experimental data used as input to the models.

Time-Dependent Phenomenon

A number of different types of reactions can cause the material properties of a polymeric composite structure to change over time. The first category to be discussed is stress or fatigue. As load is repeatedly applied to a structure, damage will initiate and grow within the structure changing the strength and stiffness of a composite. The second category is strain or viscoelasticity. The compliance of the matrix in a composite can

change with time because some deformation processes require time to occur. The change in compliance of the matrix will obviously effect the stiffness of the overall structure but in addition, a change in strength can also occur due to stresses being redistributed. A third type of change that can occur with time is chemical aging. Here the matrix of the composite chemically reacts with its environment or simply continues to cure over time effecting its physical properties. The fourth category to be discussed will be physical aging where the properties of the matrix material change due to the atomic chains in the matrix reorienting with time in a manner that does not require a chemical reaction.

Each of these effects of time change with temperature. An increase in temperature accelerates the various processes, effectively making time pass more quickly. It is the elevated temperatures that a high speed aircraft will have to endure that makes the time dependent effects on composite materials a problem for this application. Because of the way temperature effects these phenomenon, they can all be thought of as a function of both time and temperature. Finally combined effects of these time dependent phenomenon will be discussed.

Stress (Fatigue Damage)

Stress repeatedly applied to a composite structure will cause damage to the structure that initiates and grows. Fatigue is normally not thought of as a time-dependent property because it is quite a weak function of time. It is listed here because the repeated application of loads over time in the service of the material create fatigue. Also when the fatigue response interacts with the other time-dependent phenomenon that will be listed, it can become a time-dependent property.

The field of fatigue damage and the modeling of fatigue damage is quite large. A good overviews of the field can be found in the books *Damage Mechanics of Composite Materials*[7] and *Fatigue of Composite Materials*[8]. The damage progression in a

7

laminate is often started with the initiation of matrix cracking, followed by delamination, and finally fiber failure. The field is extremely complex with the damage depending on stress levels, fatigue rates, number of fatigue cycles, stress variation due to geometry, material properties, laminae orientations, and stacking sequence, just to name some of the more important influences. Of course the stiffness and the strength often termed the "residual strength," would depend on the damage state in the composite. Even the effects of the damage on strength can be a very complex function with strength at times increasing as damage develops.

Strain (Viscoelastic Deformation)

A second cause of changes in the deformation and strength of a composite laminate over time is due to viscoelasticity. Viscoelasticity is the time-dependent deformation of materials caused when mechanisms of deformation do not occur instantly but instead require some amount of time to develop. The viscoelastic nature of composite material has also been widely studied. Overviews of this subject have been written by Schapery[9] and by Dillard[10] and a review of literature conducted by Scott et al[11]. Viscoelastic deformation is often divided into two categories: linear and nonlinear, with linear being much easier to model because the effects of increments in load are additive. Viscoelasticity not only effects the deformation of a composite, but also effects the strength. As the compliance of the composite material changes, the stresses within the composite will redistribute. The change in internal stress will cause the overall strength of the composite to change. The linear visco elastic deformation is normally characterized by measuring the creep compliance of the material, that is, the time-dependent deformation of the material due to a constant stress. To relate this material property to other stress histories, a hereditary integral of the form

$$\varepsilon(t) = \int_0^t D(t - \psi) \frac{d\sigma(\psi)}{d\psi} d\psi \qquad (1)$$

is used where D is time-dependent creep compliance and ψ is a dummy time integral over

which to integrate. To solve two or three dimensional viscoelasticity problems becomes

quite difficult because of the addition of the time variable to the normal elasticity

equations[12]. In general it is either approached through a finite element formulations or

through transformations such as a Laplace transformation that takes the time variable out of

the elasticity equations. Time is introduced back into the solution through a reverse

transform. Under certain conditions, a correspondence can be established between the an

elastic problem and the viscoelastic problem of interest. In this case once the elasticity

solution is solved, the viscoelastic solution is obtained by adding a function of time.

The modeling of a composite becomes more complex because it is an orthotropic

material. Often the elastic fiber and viscoelastic matrix properties are combined in a

micromechanics model where a representative volume of material is modeled to determine

the viscoelastic deformation of a composite laminae. The viscoelastic laminae properties

are then used to predict laminate properties.

Viscoelastic deformation can also be nonlinear, where the compliance becomes not

only a function of time but also of stress level. A nonlinear response can be caused

directly due to the material response[13] or indirectly due to damage formation[14]. This

type of response is more likely at higher stress levels and near failure it can be

expected[15]. At times, nonlinear viscoelastic behavior can be accounted for by shifting the

compliance response in time according to a function of stress.

Chemical Aging

Properties of polymer composites can change due to chemical aging. This can take

on several forms. The matrix material of some composites simply continue to cure for

long periods of time[16]. These changes are usually indicated by a change in the glass transition temperature of the material. Other chemical changes can occur due to the matrix reacting with the atmosphere. The reaction is often due to a reaction with the oxygen and resistance to this phenomenon is often referred to as thermo-oxidative stability[17]. This phenomenon is usually measured by weight loss to the specimen but can also cause the material that is left behind to be brittle. Chemical reactions can also occur with other substances in a structure's environment, which for an aircraft means moisture[18] and such chemicals as jet fuel[19]. The rate of change in physical properties due to these environmental interactions not only depends on the rate of the chemical reaction but also on the diffusion rate of the agent into the material.

Physical Aging

Over time the properties of a polymer matrix composite can change due to physical aging[20]. Physical aging does not require the breaking or the forming of chemical bonds as was the case in chemical aging. With physical aging, the atoms in a material only rearrange themselves as they try to achieve a state of equilibrium. Usually this means that the atoms become more closely packed together. This process takes time since there is resistance to atomic movement. The effect of physical aging on the properties of advanced composite systems has more recently been studied by Feldman[21], by Gates and Feldman[22], and by Hastie and Morris[23]. Usually the physical aging process is characterized by a change in the viscoelastic properties of the composite over time which is reversed when the material is heated above the glass transition temperature. This process might also be expected to change other physical properties such as strength or toughness.

Combinations

Each of the time-dependent processes listed above can change the properties of a composite over time. The effects of the processes become more complicated when they simultaneously act and interact, to change the properties of composite materials. One additional complication that can also be added to the above list of time effects is a change in temperature. Each of the time-dependent processes listed above is also effected by temperature, usually with an elevation in temperature increasing the rate of change with time. Because the effects of these time-dependent phenomenon do interact with each other, studies of the interactions must also be conducted.

A logical combination study that might be conducted is the effect of fatigue while the temperature is also changing. This combination is usually termed thermomechanical fatigue (TMF). Castelli[24] studied TMF of a metal matrix composite and found that a significant difference in properties was found depending on whether stress and temperature where increased and decrease together or whether they were varied out of phase with each other. Experiments conducted by Roberts [25] showed little interaction between thermal and mechanical fatigue. Pasricha et al.[26] measured the response of a thermoplastic composite to TMF and found that the laminate became stiffer with time, probably due to physical aging. To model the deformation measured in this test, a nonlinear viscoelastic/viscoplastic model was used. Haskins and Kerr[27] combined oxidation and fatigue and found significant decrease in properties due to the combination. The lack of more studies on TMF may be an indication of the difficulty associated with running these tests.

Failure Parameters

The time-dependent phenomena described in the last section can effect the critical parameters of composites. In addition, some of the critical properties may be effected

directly by time. The critical parameters of a composite include strength of the fiber and the matrix; critical strain of the fiber and the matrix; matrix toughness; laminae strength or critical strain in the fiber direction and transverse to the fiber direction, both tension and compression; and composite toughness. Critical parameters can also be related to specific damage mechanisms of a laminate such as, onset of matrix cracking, saturation of matrix cracking, initiation of delamination, laminate buckling, etc. Because the list of critical parameters is so extensive, the review here will concentrate on only the laminae strength transverse to the fibers and composite fracture toughness. It is expected that both of these properties will be effected by the time-dependent properties of the matrix. These basic properties are also important in predicting laminate properties such as the onset of matrix cracking or delamination[15].

Transverse Composite Failure

The transverse failure of composite material can be tested in several ways. Transverse strength usually refers to a unidirectional specimen tested to failure with a constant load or strain rate. Strength can either be tested with a uniaxial tension test or with a bending specimen. Creep rupture tests are conducted on similar specimen but in this test, a constant load is quickly applied and then held constant until failure occurs. The time to failure is the critical value in these tests. Initiation of matrix cracking is also a measure of transverse failure. Here laminates with 90° plies are tested and the critical laminae properties must be calculated from the measured laminate response.

According to Whitney and Browning[28], the transverse tension strength test is the most useful test for characterizing matrix dominated failure modes. They also indicated that strain to failure was a critical parameter.

Asp, et al.[29] studied the transverse strength of a glass/epoxy composite material. A finite element micromechanics model was used to relate a matrix failure criterion to the

composite strength property. The matrix failure criterion was based on the dilatation strain energy density for cavitation base on previous study by the same authors[30]. Strength predictions from the model were made for composites with various volume fractions and included thermal stresses. The model predictions were also compared to experimental data. Yet a third study by the authors[31] showed the importance of the fiber and interphase properties on the stresses in the matrix that initiate failure.

Meurs[32] showed that the variation of fiber spacing and free edge effects significantly effected that stress field in a composite. These stresses lead to fiber-matrix debonding. The debonding was related to both debond strength and fracture toughness rather than matrix strength. The importance of interphase properties was also mentioned in this study.

Ishai et al.[33] studied the time-dependent failure of both a tough and brittle glass epoxy composites. They tested three point bending specimens with fiber orientations from 0 to 90 degrees. They found that the except for when the fiber were well aligned with the loading direction ($<10°$) the strength of the composite could be scaled to the transverse ($90°$) test results. The brittle composite was found to fail by fiber-matrix interface separation while the ductile composite was found to fail by tensile rupture of the matrix. They also found that the strength varied linearly with the log of the strain rate over the three decades of strain rate tested. The results were modeled with a polymeric rate process model suggested by Bueche[34, 35].

Govaert et al.[36] modeled the time-dependent failure in glass/epoxy transverse to the fiber. They postulated a failure criterion which relates the critical octahedral shear stress to a function of strain rate and mean stress. This criterion was proposed by Ward [37]. A finite element micromechanics model was used to relate the matrix failure to the composite properties. Composite three point bending tests were performed over three decades of strain rate. Creep tests were also performed and compared to the model.

Composite Toughness

The toughness of a material is its resistance to crack growth. In composites, cracks can grow between laminate layers. These cracks are called delaminations. Cracks can also grow within a ply along the fiber direction creating matrix cracks. Cracks do grow transverse to the fiber direction as well but this growth is hindered by the interaction with the fibers.

Berglund et al.[38], showed that the toughness of the matrix material effects the growth of delamination and the onset of matrix cracking. He also found that the toughness associated with crack through the thickness of a laminae was different from the toughness associated with growth of the matrix crack along the fiber direction. They postulated that laminae properties are better studied directly from laminates instead of from unidirectional composites because of a difference in constraint properties.

Frassine and Pavan[39] studied the fracture toughness of neat resin and composite material. In their work on a polyetherimide composite, they found that toughness is relatively insensitive to rate and temperature. They further found that composite toughness was significantly lower than the neat resin toughness and also differed in how it varied with time and temperature.

You and Yum[40] studied the effect of loading rate on delamination toughness in a graphite epoxy composite. They found that delamination toughness increased with delamination propagation speed at higher rates of speed but remained fairly constant at low rates.

Knauss[41] reviewed the time-dependent fracture mechanisms in polymeric material along with the models to describe them. In this review he summarized some of his own work[42] where it was postulated that fracture energy and crack opening displacement

may remain constant. These assumptions were compared to experimental results of an polyurethane elastomer with good agreement.

Kim and Stone[43] studied how different path independent integrals used to characterize the state of a crack tip in viscoelastic/viscoplastic medium might be used to describe the effects of time, temperature, and load on crack growth. They identified restrictions on the various integrals in situations involving unloading , temperature changes, or composite materials.

Schapery[44] used a correspondence principle to relate a path independent integral of a elastic problem to a fracture parameter for a corresponding viscoelastic problem. The parameter designated W_f has a physical interpretation of the mechanical work available to extend a crack tip supplied by the surrounding viscoelastic medium. This parameter is only valid for crack initiation because the boundary of the problem must remain constant. The analysis holds for a composite material where the boundaries within the composite are parallel to the direction of crack growth. The author [45] also investigated path independent integrals for viscoelastic material where crack growth was allowed. The calculation the these parameters were not simplified by the existence of a corresponding elastic problem.

Yoon and Allen[46] investigated a cohesive zone model to describe crack growth in a composite material. This model allows unloading and crack growth but is limited by the ability to measure the necessary constitutive properties of the material in the cohesive zone.

Accelerated Testing

The expected life of composite materials in many applications is quite long and properties of the material are expected to change over that time due to the factors discussed previously. In the application of interest here, a high speed commercial aircraft, the material is expected to last for 20 years with 60,000 hours of that time at elevated temperature. It is

impractical to run tests which last for this period of time. Even if tests could be performed for such long periods, the knowledge of how the material will behave is needed now to design the aircraft. Assuming advances in material science, the materials of interest for use on planes designed 20 years from now will be completely different from the materials that one might start testing today. For these reason accelerated tests for the time-dependent effects must be developed.

Acceleration of fatigue is normally accomplished by increasing the frequency of loading. This generally works well as long as other time-dependent phenomenon such as viscoelasticity, or oxidation do not interact with the fatigue response. Haskins and Kerr[27] used this technique to reduce test times by a factor of 120.

Acceleration of the other phenomenon is more difficult because their effects are much more directly a function of the time. Accelerated testing of viscoelastic deformation is well established, and usually accomplished using time-temperature superposition[47]. Here elevating the temperature is used to effectively accelerate time. The difficulty with any accelerating scheme is to establish the relationship between the accelerated test the non-accelerated. With time-temperature superposition, compliance measurements are made over a short time period at several different temperatures. These compliance measurements are plotted against the log of time. It has been found that the compliance measurements can be shifted on the log time scale to form a smooth curve called a master curve as shown in Figure 1. This curve predicts the compliance of the material over a larger time range than was actually tested. The amount of acceleration provided by a given elevation in temperature is established by the overlapping of the compliance curves measured at the different temperatures.

To form the master curve, one curve remains stationary and all the other curves are shift to it. It is the temperature associated with the first curve for which the master curve predicts time-dependent deformation. By recording the time shifts required to form the
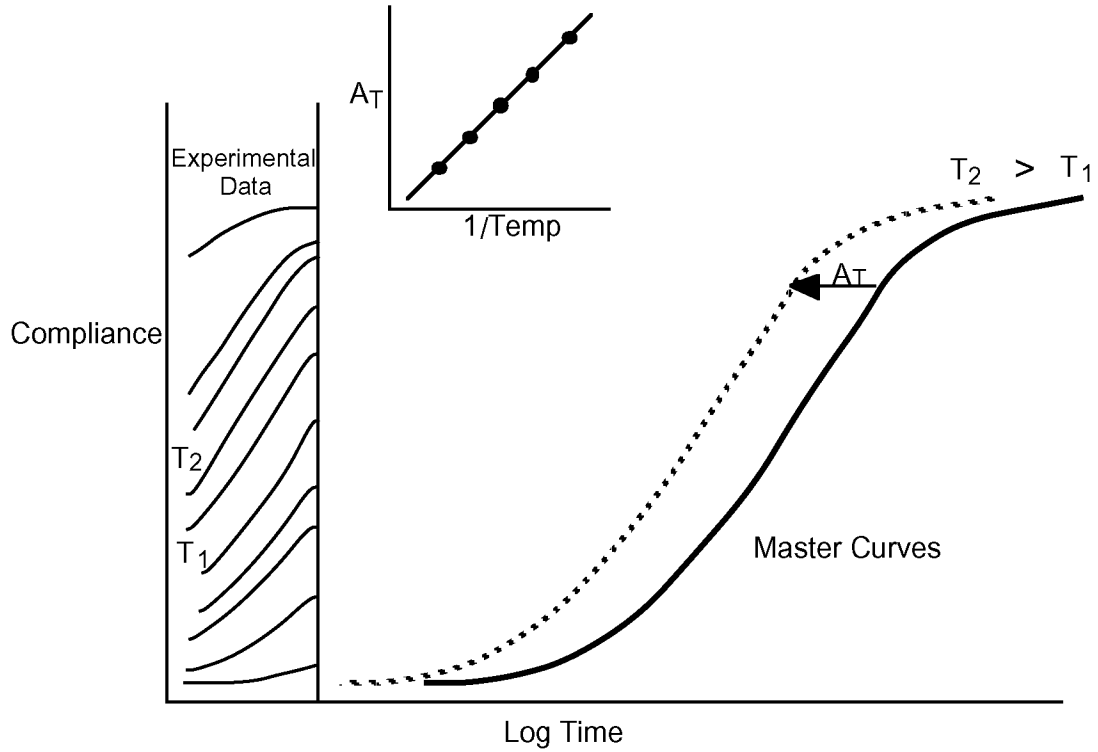
Figure 1. Time-temperature superposition and the formation of a master curve.

master curve which are usually referred to as shift factors (A_T), a relation between the horizontal shift and temperature is established. This relationship can be used to shift the entire master curve to other temperatures. Using the master curve shifted to the appropriate temperature, creep compliance over many orders of magnitude can be predicted. Time-temperature superposition was developed for polymers but it has been successfully extended to the deformation properties of polymeric matrix composites[12, 48].

Models for how the shift factor A_T should change with temperature have also been developed. Williams et al.[49], developed the following relation for A_T which is found to work well above T_g.

$$log\,A_T = \frac{C_1(T - T_0)}{C_2 + T - T_0} \qquad (2)$$

17

where C_1 and C_2 are material constants and T_o is the reference temperature for the master

curve. Below T_g, the value of A_T is often found to relate to $1/T_R$ were the subscript R

indicates that the temperature must be expressed as absolute temperature, °R.

$$log\,A_T = \eta\left(\frac{1}{T_R} - \frac{1}{T_o}\right)$$
(3)

where η is the shift constant. This relation is predicted for Arrenhius type rate processes

which is described by the equation

$$r = A\,e^{\left(\frac{-\Delta H}{R T_R}\right)}$$
(4)

where r is the rate of the process, ΔH is the activation energy, R is the ideal gas constant,

and A is a material constant. The temperature in the preceding equation must be expressed

as an absolute temperature such as °R. Shift factor variation over relatively small

temperature ranges have been adequately described with a linear function.

$$log\,A_T = \alpha(T - T_0)$$
(5)

where α is the shift rate.

Lohr[50] created master curves from the yield data of several neat resin systems but

found that the shift factors were quite different from those obtained from stress relaxation

tests.

Moehlenpah et al.[51], used time -temperature superposition to create master curves

of strength for a glass/epoxy composite. The shift factors used to create the master curves

were obtained from modulus data. They found that the shift factors for the composite

strength was not effected by type or orientation of the glass filler nor was it effected by the

mode of loading even though the actual strength values were different.

18

Miyano et al.[52, 53], also used the time-temperature superposition to describe changes in strength with time and temperature. The superposition method was shown to apply to the strength properties of a unidirectional thermosetting epoxy based composite in tension, compression and bending, and in both the longitudinal and transverse directions. In some cases, the shift factors for strength were shown to be similar to the shift factors measured from compliance results. Careful examination of the test results revealed that the shift factors obtained below T_g were rather arbitrary. The data could have been shifted with much different shift factors such that a smooth master curve was still attained. The different shift factors could be used to make time to failure predictions that differed by several orders of magnitude. Part of the problem was that the tests at a given temperature were only tested over three decades of time which did not allow much overlap of the constant temperature curves during the formation of the master curve. The region below T_g, which produced the most ambiguous shift factors, is the only region of interest for most structural materials because above the T_g, materials are usually too compliant. The results in this study were for a thermosetting composite while many of the composites of interest for advanced aircraft are thermoplastic which often behave in fundamentally different ways. Although the use of the compliance shift factors for strength would be extremely helpful for making accelerated strength prediction, it is not clear from this study that it will be accurate, especially for the thermoplastic composites of interest. Miyano et al.[54], extended the approach to fatigue strength of a woven composite with reasonable results.

Pride et al.[55] have also attempted an accelerated strength study of creep rupture of a polyimide resin. They used a Larson-Miller parameter[56] to relate rupture time tested at different temperatures. The Larson-Miller parameter is given by the expression

$$T_R \left(C + log\, t \right) \qquad (6)$$

19

where T_R is temperature in $^{\circ}R$, t is the time to rupture, and C is a material constant. This expression is based on assuming that rupture is an Arrenhius-type process and described by Equation 4.

Brinson et al.[57], created an accelerated test methodology for creep rupture of composites. This methodology assumed that the shift factors for rupture would be the same as for compliance and further assumed that the strain to failure during the rupture test would stay constant. They compared the model to the result of a graphite epoxy composite with good results. They also looked at a Larson-Miller parameter and reported a poor correlation with experimental results.

Frassine and Pavan[39] used a time-temperature-superposition method to make accelerated predictions of toughness. They used shift factors obtained from neat resin strength data to shift both neat resin and composite toughness data into a master curve.

Acceleration of chemical aging is not as well established but often involves an elevation in temperature and an increase in the concentration of the agent which is chemically reacting with the matrix[19].

Struik[20] was able to predict the long-term effects of physical aging using a method similar to the time-temperature-superposition method described earlier. He was able to shift the compliance curves at a given aging time to form a master curve. He found that the rate with which the compliance curve shifted remained constant with aging time at a given temperature. By assuming the rate would remain unchanged over long periods, extended predictions could be made. One complicating factor was that a material would continue to age as a compliance specimen was tested. To model this, real time during which aging occurred was related to an effective time where aging remained constant. This method of accelerated testing of long-term physical aging was extended to composite systems of interest to the current application by Gates and Feldman[22].

Brinson[15] outlined a accelerated test method in which the super-position technique first used with temperature and then used with physical aging might be extended to incorporate the combined effects of temperature, aging, moisture, and stress. Once the model is created for a laminae, lamination theory can be used to extend it to laminate response. The experiments needed to support such a combined model have not been performed.

Background Summary

It is clear that in order to design an advance high speed aircraft using composite materials, accelerated test methods will be needed to support models which can predict the combined effects of fatigue, viscoelastic deformation, changes in temperature, chemical aging, and physical aging on the failure properties of these laminates. These models will be based on critical properties such as the transverse strength and toughness of the laminae. No consensus on the controlling mechanism for these properties seem to exist. The effect of time on these properties are therefore more difficult to predict. Most acceleration methodologies involve the use of elevating the temperature to speed the effects of time. Correlating an elevation in temperature to a comparable acceleration in time effects is of critical importance. The elevation in temperature may be combined with other methods such as an increase in load frequency or an increase in chemical concentration to speed specific degradation mechanisms. Much work has been conducted toward these types of acceleration methods, but very little of it was on the types of thermoplastic composite systems being considered for the high temperature applications of current interest.

A study of accelerated strength testing of a thermoset composite has been developed that applies the shift factors from compliance tests to strength results. These results however were not definitive and may not apply to the thermoplastic composites of

interest. If the shift factors for strength are the same as for compliance, this may lend insight into the mechanism behind the failure and therefore into the effect of time on failure. With this type of understanding accelerated strength predictions could be made with greater certainty.

CHAPTER III

EXPERIMENTAL PROCEDURES

This chapter describes the materials and experimental techniques used in the dissertation research. The material used for this study is a thermoplastic composite with designation IM7/K3B. The tests performed on the material include 90° tension strength tests and double cantilever beam (DCB) delamination fracture tests. Both sets of tests were run over a range of elevated temperatures and loading rates.

Material

The material used in this dissertation project is IM7/K3B. It is a graphite composite made from IM7 graphite fibers and K3B, a thermoplastic resin. The IM7/K3B material was chosen because this is a material being considered for high speed aircraft[19], where delayed failures are a possibility because of the extended service time of the composite material at elevated temperatures.

The IM7 fiber is a fairly common high strength graphite fiber manufactured by Hercules, Inc. made of 5 micron fiber filaments with a modulus of 40 Msi and tow strength of 785 ksi[58].

The K3B matrix is an amorphous thermoplastic polyimide resin. Polyimide polymers can be formulated as a thermoset through an addition reaction or as a thermoplastic through condensation. The highly proprietary K3B resin is a slight processing variation on a more widely reported resin designated as K_{III}. K_{III} is made through a condensation reaction and is a combination of a pyromellitic dianhydride, and a diamine where the bulky diamine acts to prevent crystallization[59]. The reported modulus and strength of K_{III} are 546 ksi and 14.8 ksi, respectively, and K3B is expected to be similar[59]. The T_g of K3B has been published to be 457°F [21].

The K3B resin material has been shown to physically age[21]. Figure 2 shows how the compliance of K3B changes with various amounts of aging. From this graph, it is clear that the physical aging phenomenon can significantly effect the properties of this resin and therefore the properties of composites made from the resin.

IM7/K3B is a candidate for such applications as the structural material for high speed aircraft because the high T_g of the resin should allow the composite to maintain its strength and stiffness at the elevated temperatures expected for these applications. Published values of stiffness for this material are 24.2 Msi parallel to the fibers and 1.21 Msi transverse to fibers. The strength of the composite has published values of 234.8 ksi
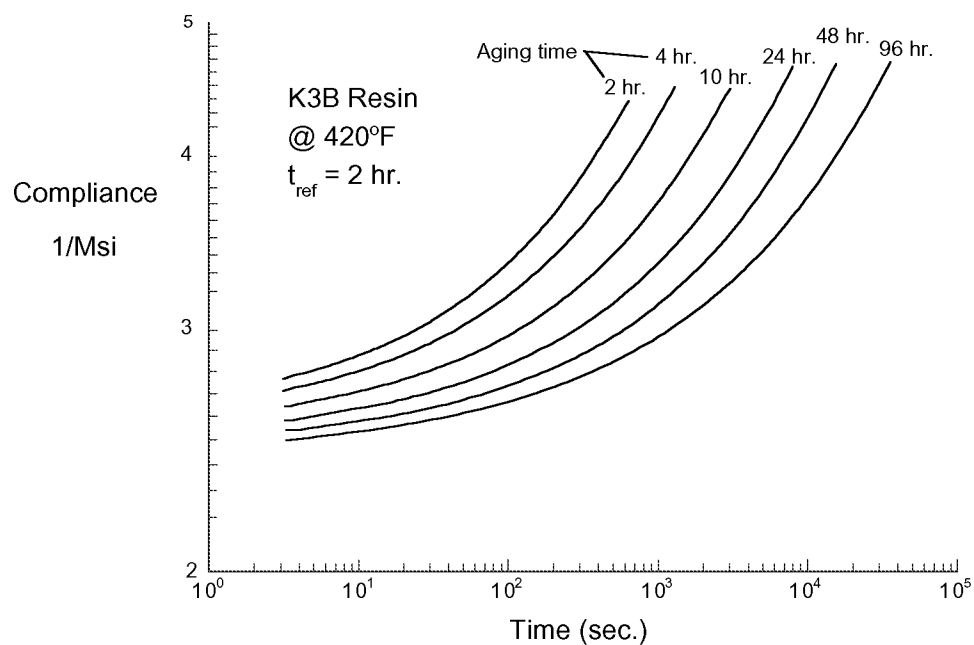
Figure 2. Aging of K3B resin as shown by momentary master curves[21].

24

in the longitudinal direction and 6.96 ksi in the transverse direction. These properties are for room temperature conditions using standard test methods which are performed over relatively short time scales[6]. These properties of course are not constant and should be expected to change as temperature and time scale change.

Two types of laminates were prepared from the IM7/K3B prepreg material. Four panels measuring 12 in. x 24 in. were prepared with all 8 plys oriented with the fibers running in the 24 in. direction. After these panels were cured using the manufacturer's recommended cure cycle, each panel was cut into 30 test specimen measuring 1.5 in. x 6 in.

a) 8 ply laminates
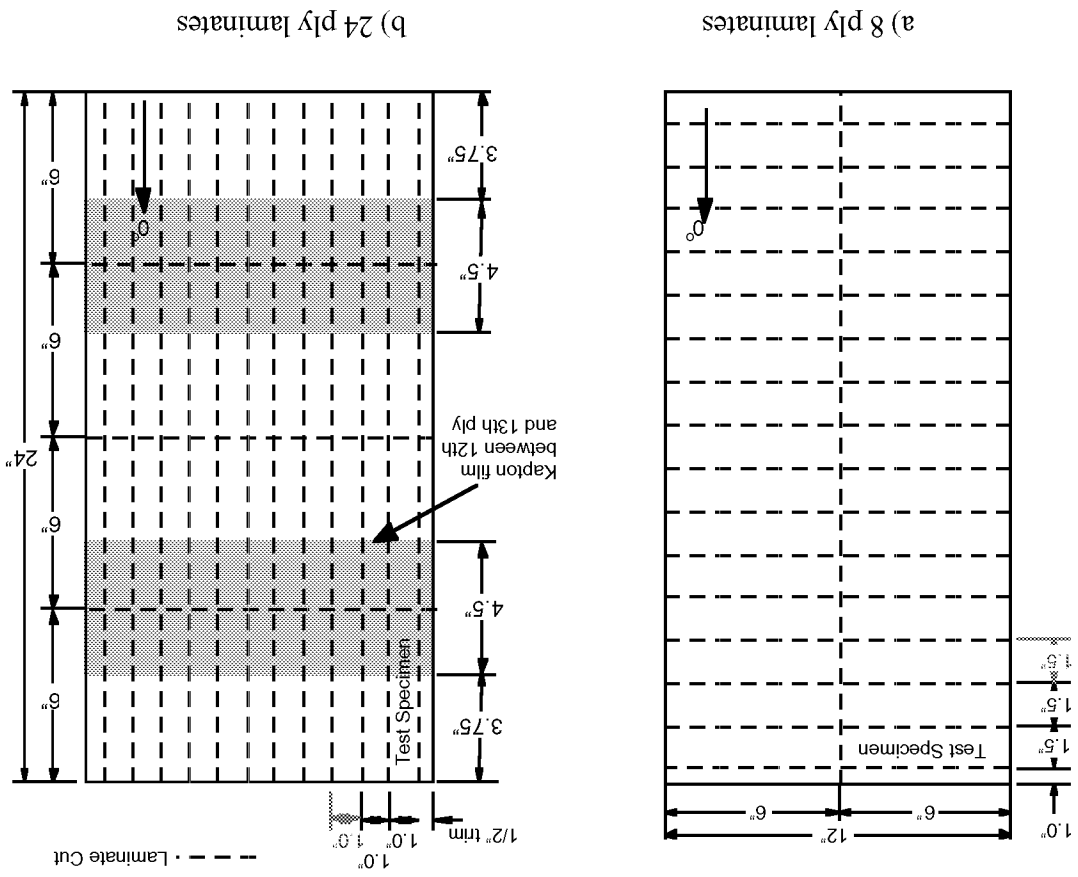
b) 24 ply laminates

Figure 3. Test specimen layout on the K3B composite laminates.

as shown in Figure 3a. A second set of laminates were manufactured using as 24 ply

laminates. These panels had 0.002 in. Kapton strips inserted between the 12th and 13th

plies. These sheets of Kapton were sprayed with a mold release agent so that the Kapton

did not bond to the composite during the curing process thus creating artificial

delaminations within the laminate. The position of the Kapton strips can be seen in Figure

3b. After curing with the manufactures recommended curing cycle, each panel was cut into

1 in. x 6 in. test specimens as seen in the figure.

Transverse Strength Tests

Transverse strength tests were performed at temperatures between 300°F and 450°F

over a range of time scales so that time to failure ranged from 0.5 sec. to 24 hrs. During

the tests; load, displacement, and strain readings were recorded.

The test specimens for the transverse tension tests are shown in Figure 4. The test

specimens are cut from the 8 ply panels and are around 0.044 in. in thickness. The test

specimen are cut from the laminates so that the fibers run transverse to the loading

direction. Three strain gauges are attached to each specimen as shown in Figure 4 and are

arranged so that the bending front to back, bending side to side and average strain could be

determined. The strain gauges which are manufactured by Micro Measurements Co. and

have a 1/4 in. gauge section are designated WK-00-250BG-350. Although they are only

designed for temperatures up to 350°F, they were found to be adequate for the tests that

were conducted in this project up to 450°F. A rather complicated bonding procedure was

used to apply the gauges. The specimen were first lightly sanded in the area where the

gauges where to be applied. A thin layer of M-Bond 600 adhesive was then applied and

the specimen was heated to 250°F for one hour to cure the base adhesive layer. A second

layer of adhesive was applied as the strain gauge was bonded. The gauge was clamped to

the specimen to hold it in place, and the specimen was heated again to 250°F for one hour.
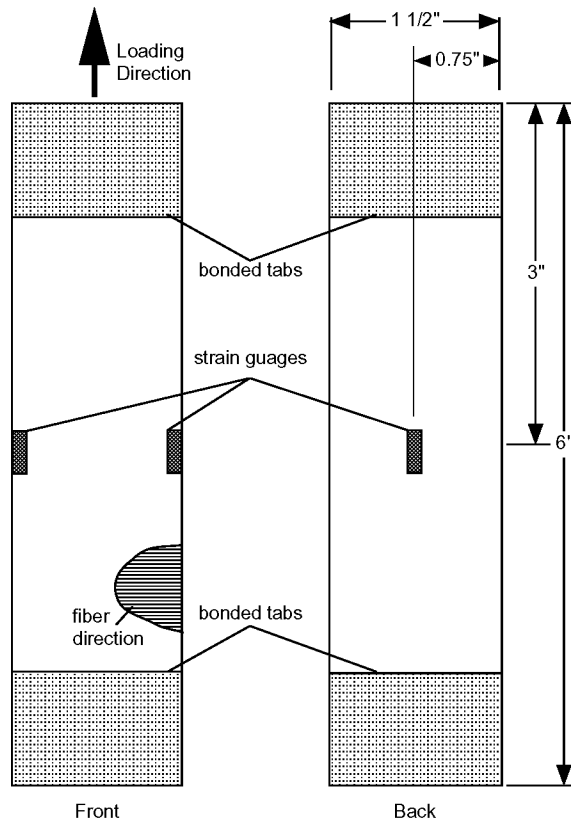
Figure 4. Transverse tension test specimen.

After the strain gauges were applied to the specimen, the loading tabs were applied. The loading tabs were used to reduced stress concentrations due to clamping during the tension tests. The loading tabs were applied to each end, front and back, and measured 1 in. in length. The width of the tabs matched that of the specimen at 1.5 in. The tabs were made from 220 grade open weave silicon carbide sand paper manufactured by 3M. The open weave sand paper was infused with an epoxy resin. The resin was made by the Hysol Division of the Dexter Corp. and had a designation of 934NA. The 934NA resin is a two part epoxy that was chosen for its ability to withstand high temperatures. The two parts of the epoxy were mixed in the ratio recommended by the manufacturer and had a consistency

similar to thick molasses. A thick layer of the resin was applied to sections of the specimen that were to receive the tab material. The tab was then placed onto the adhesive layer and a second layer of resin was applied so that the open weave mesh was completely infused. Plastic sheets that had been sprayed with mold release agent were placed on either side of the specimen. Each end of the specimen was then placed in a clamp with flat faces which were constrained to remain parallel. The clamp held the mesh material in place and insured that the surface created by the dried epoxy would be flat and parallel. The grit mesh material caused the tabs to be a constant thickness and created a rough grit surface that could be easily gripped. The epoxy was allowed to cure overnight.

Moisture was then driven out of the test specimen with a standard drying cycle. After drying, the specimen were placed in a 400°F oven for 4000 min. (66 hrs.). This aging cycle was conducted in an attempt to keep aging from skewing the test results. Although changes in physical properties caused by aging of this material seems unavoidable, it was not the focus of this investigation. The aging results shown in Figure 2 indicate that the effect of the first increment of aging is more significant than subsequent increments of equal length. The test specimen were uniformly aged for a period that was significantly longer than any of the anticipated tests. This should have created a uniform state of aging that would not significantly be effected by the additional aging that would occur during the tests, which are conducted over different time periods. Thus, although all the test specimen will be effected by aging, they will all be similarly effected. After each specimen was prepared, it was stored at 225°F for less than a week before being tested.
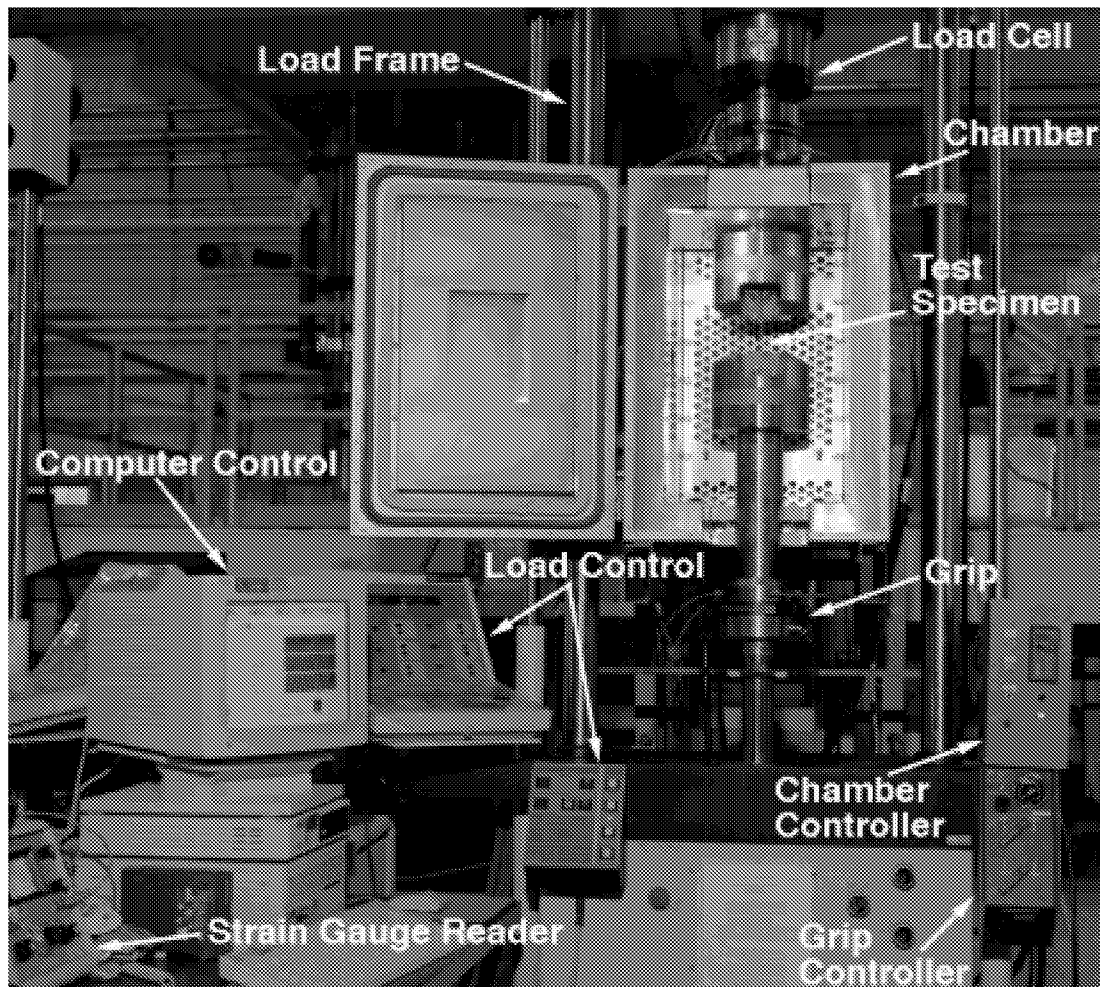
Figure 5. The test apparatus used during transverse tension tests.

The transverse strength tests were performed in a hydraulic load machine. The test set up can be seen in Figure 5. The 22 kip test machine is made by Instron Corp. and is model 8500. The controller of the hydraulic load frame monitors both load measured by the 22 kip load cell and position measured by an LVDT (linearly variable displacement transducer) located within the test machine. The controller is capable of controlling either the load or the displacement of the test machine. The test machine is equipped with an environmental chamber which surrounds the test section. The model 651 chamber is

manufactured by MTS Corp. and has its own temperature controller. It is capable of creating test environments from -200°F to 600°F. The test machine connects to the test specimen through hydraulically actuated wedge grips. These grips designated as model 647 are manufactured by MTS Corp. and are specially designed for elevated temperature testing. They are designed so that the water cooled hydraulic actuators remain outside the environmental chamber since hydraulic oil is not capable of withstanding the high temperatures. The hydraulic actuators connect through mechanical linkages to the wedges inside the oven that move to clamp the ends of the test specimen. A grip controller mounted on the load frame opens, closes, and controls the pressure of the grips.

Both temperature and strain were measured during tests. The temperatures, both inside and outside the chamber, were monitored using a "Digi-sense" scanning thermometer manufactured by the Cole Palmer Co. capable of reading 12 type T thermocouples every 4 sec. Each strain gauge was monitored using a Bam 1 bridge amplifier and meter manufactured by Measurements Group. Each gauge was connected in a quarter bridge configuration.

All instruments were connected to the test computer. The original Macintosh IIci was upgraded to a Macintosh Quadra 700 during testing. The computer was configured with two boards made by National Instruments Corp. The first was an GPIB computer interface which was used to send commands to the hydraulic load frame. The second was a multifunction I/O board which read voltages. Two voltage inputs came from the hydraulic load frame and were monitors of load and displacement. Three voltage inputs came from the three strain gauge readers. A final input was from the thermocouple reader and was made through the standard modem port. The computer read, processed, plotted, and stored the data, and sent appropriate control commands to the load frame based on the processed data. This complex data acquisition and control system was controlled by a Labview program also made by National Instruments Corp. Labview is a versatile programming language type application with commands to process data and control digital equipment. To run the experiments for this study, a complex computer program was written within Labview to coordinate all the various functions that were needed. Labview computer programs are somewhat unusual in that they are graphical instead of existing as lines of code. Figure 6 shows a small section of the code which looks more like a electrical diagram than a computer program. The lines represent flow of data while other symbols represent do loops, branch points, subroutine calls, etc. The computer program interacts with the researcher through windows on the computer screen. An example of how the computer screen might look while running a test is shown in Figure 7 and shows buttons used to turn various functions on and off, boxes to enter data, boxes to display results, and windows to plot data. The computer controller was able to read and record to disk over 200 sets of data/sec while performing other tasks.
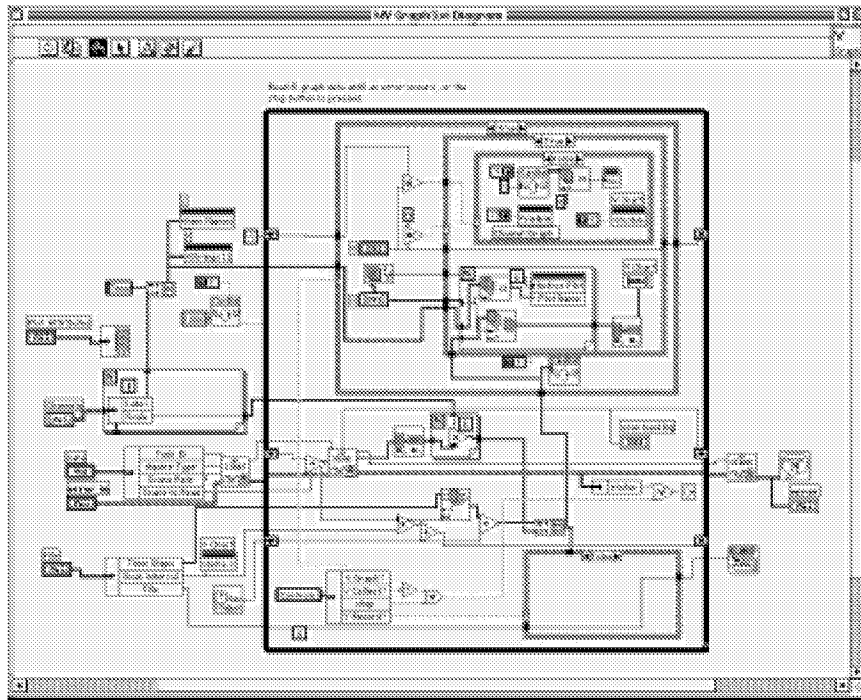
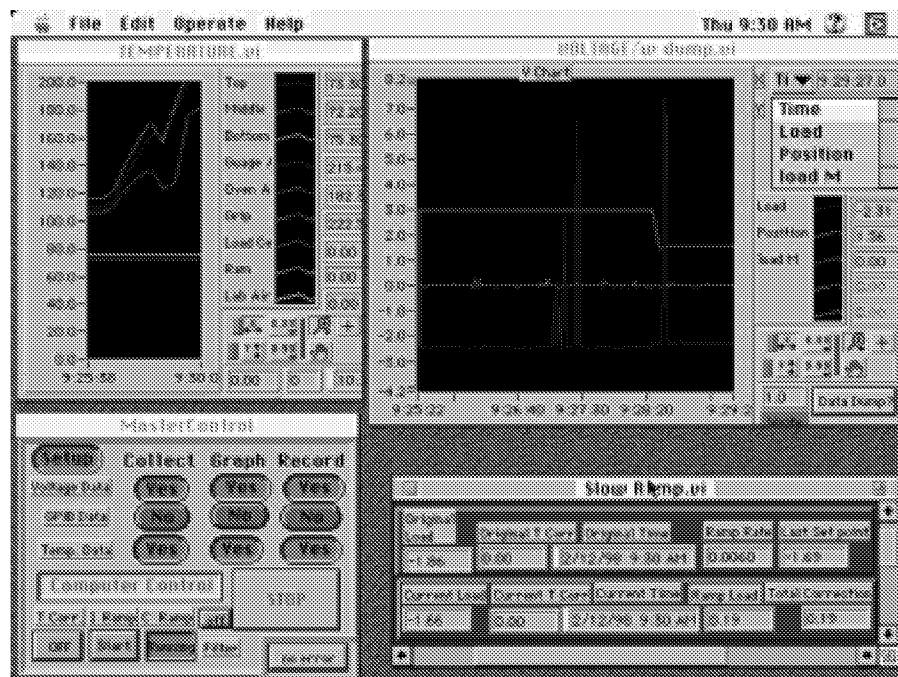Figure 6. An example of the Labview computer code.

Figure 7. An example of the Labview computer display while performing a test.

32

Transverse strength tests were performed at four temperatures: 300, 350, 400, and 450°F. At each temperature, constant load rate tests were performed with a range of loading rates that produced failure times from half a second to approximately 24 hrs. The five ramp rates that were chosen were 500, 25, 1, 0.05, and 0.0025 lb/sec. These rates were chosen to be fairly evenly distributed when plotted on a logarithmic scale. At each loading rate and temperature, three or more duplicate tests were performed.

To perform these tests, the test specimen from the 8 ply laminates were put in random order and the specimen were then tested in that order. The dimensions of the specimens to be tested were first measured. The width and thickness of the specimen were measured to the nearest 0.0001 in. using micrometers at three different positions spaced along the length of the test specimen. The average of the measurements was recorded for the thickness and width. Strain gauges were then applied followed by the end tabs, as described earlier. The specimen were aged and stored until they could be tested. Prior to performing a test, the test machine was heated to the test temperature and allowed to reach equilibrium. This could take many hours because of the large mass of the grips. Once the test environment was at the desired temperature, a specimen was taken from the storage oven and gripped in the upper hydraulic grip. The specimen was gripped so that a quarter of the tab extended out of the hydraulic grips. The specimen was centered in the grip side to side in both the upper and lower grip so that it was well aligned with the test machine. The specimen was not gripped by the lower grip at this time. The three strain gauges were connected to the three strain gauge readers. The oven door was closed and the specimen was allowed to heat up to the test temperature. The temperature of the specimen was monitored by thermocouples located near each grip and at the center near the strain gauges. The specimen was heated for 30 min. to allow temperatures to equalize. Once the specimen, which was hanging from the upper grip was at temperature, the strain gauges were zeroed since their readings had changed significantly with the change in temperature.

33

The lower grip was then clamped so that the lower tab extended out of the grip by a quarter inch. As the specimen was gripped the control of the load frame was changed from position to load control and a small 2 lb. preload was applied to the specimen. This procedure prevented any significant overloading during the gripping process and avoided oscillation that can occur at zero load. The hydraulic pressure to the wedge grips was set to around 100 psi which was about as low as it could be set. The low grip pressure, the extending of the tabs out of the grip, and the tabbing procedure were all carefully chosen details to help avoid a stress concentration at the grip which would cause premature failures. After the specimen was gripped, it was ready to be tested.

The constant load rate tests were generally controlled by the hydraulic load controller which has advanced feedback signal processors which allow it to perform tests well at high rates of speed. The hydraulic load controller however only performs a loading rates down to .003 lb/sec so, for the slowest test, the loading rate was controlled by the test computer. The test computer calculates a load given a constant ramp rate and starting point and sends this as a constant set point to the hydraulic load controller. By updating the load every few seconds during a 24 hr. long test, a constant load test is achieved.

The computer interface with the hydraulic controller was important for another reason. It was found that the zero point of the load cell was significantly effected by load cell temperature which is effected by the ambient lab temperature and by the environmental chamber heating. The fluctuation in the lab temperature is especially large because the heating and cooling is turned down at night. Because the longer test run for 24 hrs., they would naturally see this change in temperature. It was found that the zero point of the load cell could change by as much as 50 lbs. due to the change in temperatures that the load cell would see. This was a significant error for the tests that were to be conducted. The change in load with load cell temperature was measured and found to be a linear function. Once this correction function was known, the temperature of the load cell could be measured, and

34

a correction to the load reading could be made. By correcting for temperature, it was found that the zero point could be held constant within a few pounds. Since the load cell changed temperature slowly, no correction was needed for the shorter tests. For tests that would take an hour or longer, the temperature of the load cell was measured by the thermometer reader and sent to the computer. The computer calculated the correction and changed the set point of the hydraulic load controller by the appropriate amount. This ensured a truly constant loading rate. The measurement of ultimate load could be even more accurately measured, since an instant after failure, the load cell was in an unloaded condition. For each test the load measured after failure was used as the zero load point and this value was used to correct the other load readings for that test.

During a test; load, position and the three strain gauge readings were recorded along with temperature data. At least 100 data points were recorded while each specimen was being loaded to failure.

After each test, average strain from the strain gauge was plotted as a function of load. The difference in the readings of the gauges on the edge of the specimen was also plotted along with difference between the center gauge and the average of the edge gauges. The difference in the edge gauges is a measure of bending side to side while the difference between the center gauge and the edge gauges is a measure of bending front to back. The values of these bending strains generally stayed below 200 $\mu\epsilon$ which is less that 5% of the

average strain at failure and indicates that the specimen were well aligned. The maximum load from each test was recorded as well as the maximum average strain and the slope of the initial linear portion of the loading curve. All load values were corrected by the zero load point recorded just after failure as described earlier. The maximum load value was divided by the specimen area (width x thickness) to obtain the specimen strength.

Double Cantilever Beam Tests

The double cantilever beam (DCB) delamination tests were performed at temperatures between 300°F and 400°F over a range of time scales so that time to failure ranged from 0.5 sec. to 24 hrs. These are similar test conditions to the 90° tension tests except that DCB tests at the highest temperature , 450°F, could not be performed. During the tests; load displacement and temperature measurements were recorded. During some of the tests, video images of the delamination growth were also recorded.

The DCB specimen is shown in Figure 8. The 24 ply specimen are approximately 0.12 in. thick and are cut so that the Kapton film forms an artificial delamination at one end. Aluminum hinges are adhered to the delaminated end of the 1 x 6 in. specimen as shown in the figure. Finding an adhesive that had sufficient strength at the test temperatures was a problem. The 934NA epoxy used in the tabbing of the transverse tension specimens proved inadequate for this application. Several high temperature adhesives were investigated with no candidate having sufficient strength once it had endured the time at temperature that the test specimen would see. The best candidate was
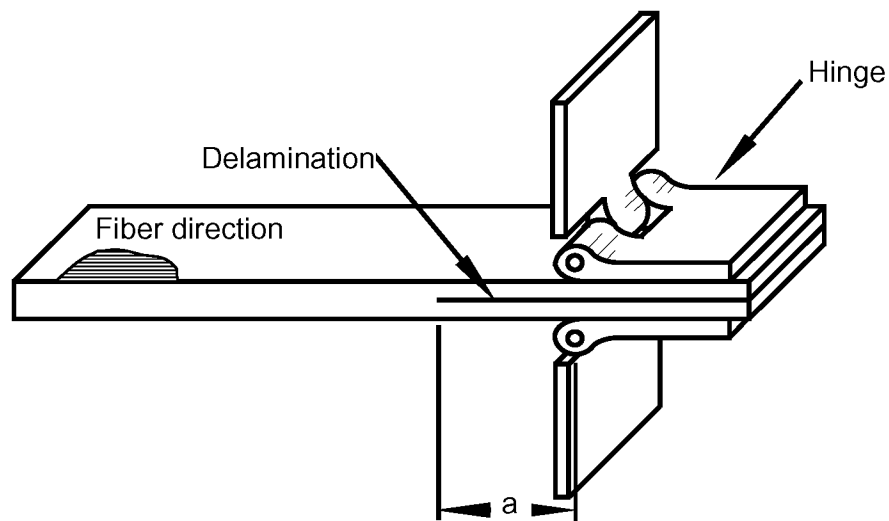
Figure 8. The DCB test specimen.

found to be a film adhesive designated HT 435 made by American Cyanamid Co. This epoxy-phenolic adhesive with a glass cloth carrier fabric was found to hold adequately if it was not held at temperature for too long. The DCB specimen were dried and aged using the same thermal conditioning cycles described earlier for transverse tension specimen. The loading tabs however were not bonded to the specimen until after the specimen were conditioned, thus keeping the time at elevated temperature on the adhesive low. The loading hinges were applied to the specimen using a jig so that the hinges would be well aligned with each other. The axis of the hinges was kept perpendicular to the length of the specimen, and the center of the hinge pin was located 1.5 in. from the end of the Kapton film. Once the hinges were placed in position with a layer of the adhesive film between the hinges and the test specimen, a clamp was applied, and the specimen was heated to 340°F for 40 min. to cure the adhesive. The specimens were stored at 225°F until they could be tested.

The test apparatus for the DCB was the same as that previously described for the transverse tension test with several modifications. First a new low capacity load cell was added to the system. This was necessary because of the low loads required to fail the DCB specimen. The new load cell was a 1000 lb. load cell manufactured by Eaton Corp. and was found to not require the temperature correction that the larger load cell had needed. A second modification was that the top hydraulic grip was removed and replaced with an extension rod that attached to a mechanical grip. The mechanical grip which clamped to the top hinge of the specimen can be seen in Figure 9. The large mass of the hydraulic grip
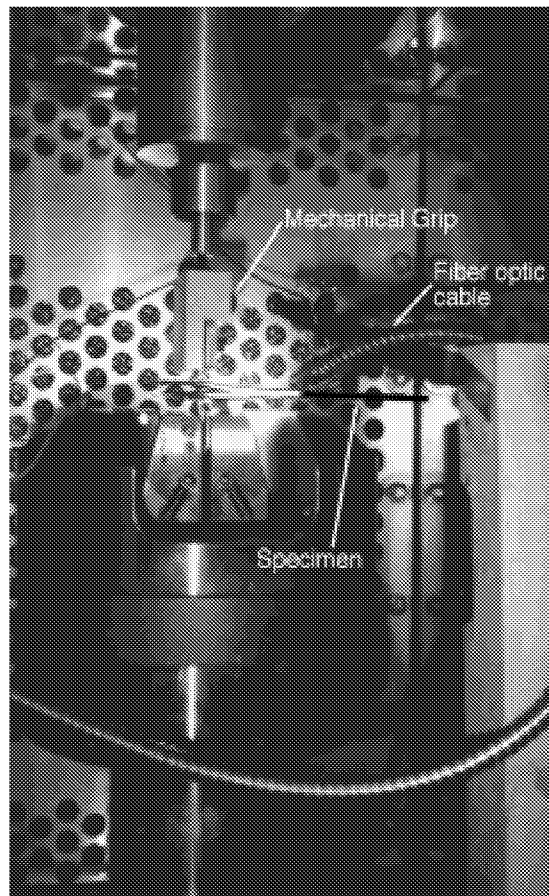
Figure 9. Photograph of a DCB test in progress.

allowed the control of the test stand to easily fall into unstable oscillation as the grip acted

as a battering ram against the load cell. Replacing the hydraulic grip with the much lighter

mechanical grip greatly improved this problem. The extension rod was water cooled to

thermally isolate the load cell from the environmental chamber and was equipped with a

ball and socket joint at the end making the fixture largely self aligning. The bottom

hydraulic grip was kept. It did not cause the problem that the top grip caused since it was

not directly connected to the load cell. Keeping the bottom grip allowed the gripping of the

specimen to be controlled from outside the environmental chamber. The strain gauge

readers were not needed for these tests.

Figure 10. The test apparatus used during DCB tests.

During some of the tests the delamination growth was observed. To see the delamination tip a long focal length microscope was used as seen in Figure 10. This microscope made by Questar Corp. has a 14 in. focal length so the microscope can focus on the crack tip through the window on the environmental chamber. The microscope is equipped with a video camera which sends the image to a monitor. The image when viewed on the 13 in. monitor is magnified by approximately 150X. A date and time stamp is placed on the image so that images can be synchronized to load and displacement data and is recorded on a standard VCR. The long focal length microscope is mounted on a moveable stage so that it is possible to follow an advancing delamination. To observe the specimen with the long focal length microscope, a high level of illumination was needed. A remote light source with a high temperature fiber-optic cable was used to obtain sufficient lighting of the specimen in the environmental chamber.

Delamination tests were performed at three temperatures: 300, 350 and 400°F. Tests were also attempted at 450°F, but the tests did not fail by delamination extension and are therefore invalid. Compression failure of the material on the surface of the specimen near the delamination tip caused these premature failures. At each temperature, constant load rate tests were performed with a range of loading rates that produced failure times from 0.5 sec to approximately 24 hrs. The five loading rates were 60, 3, 0.12, 0.006, and 0.0003 lb/sec. These loading rates are quite different from the transverse tension tests because the load to failure of the specimen are quite different. They were chosen to create failures in approximately the same time periods as the transverse tension tests. At each loading rate and temperature, five duplicate tests were performed.

To perform these tests, the test specimen were put in random order as described for the transverse tension specimen. The dimensions of the specimen were measured using micrometers and the average of three readings along the length were recorded for both thickness and width. The specimen were subjected to the drying and aging thermal cycles.

40

The hinge tabs were then bonded, and the adhesive cured. The specimen were stored for less than a week at 225°F until they could be tested. If the delamination growth was to be visually observed, a thin layer of white correction fluid was applied to the specimen in the vicinity of the delamination tip so that delamination tip could be more readily seen. The specimen was then attached to the top mechanical grip. The specimen was centered side to side in the bottom grip and was allowed to rest on the bottom grip so that specimen laid perpendicular to the loading direction. The specimen remained ungripped and the oven door was closed. The specimen was heated for 30 min. in the preheated oven to allow the specimen to equalize at the test temperature. The specimen was then gripped in the lower grip as the mechanical controller was switched from position to load control with a 2 lb. preload. The DCB specimen was then ready to be tested.

The constant load rate tests had to be run in several different ways depending on the loading rate. Tests with 0.12 and 3 lb/sec loading rates were controlled by the mechanical controller in load control mode. Because the hydraulic load controller could not perform the very slow loading rates, the 0.006 and 0.0003 lb/sec tests were performed with the test computer controlling the set point as described for the transverse tests . A new problem occurred with the fastest DCB tests. To perform the fast loading rates, the response rate of the test machine needed to be increased. The response of the test machine could be increased by "tuning" the PID control parameters on the test machine. Unfortunately, before the necessary response rate was achieved, the load machine would go into unstable oscillation. This problem was due to the combination of the high compliance of the test specimen, the weight of the mechanical grip, and the noise in the load cell signal. To solve this problem, the fastest tests were performed in displacement control. There is no difference in displacement control and load control as long as the compliance of the specimen is constant. These were the fastest tests so the specimen responses were the most constant of the tests. A displacement rate of 0.4 in/sec was chosen to achieve a

loading rate of approximately 60 lb/sec for these specimen. The exact loading rate was determined from the measured load response of each test.

During a test, load and position were recorded along with temperature data. At least 100 data points were recorded while each specimen was being loaded to failure. After each test, the distance from the center of the hinge pin to the end of the delamination insert is recorded as the delamination length, a. The delamination length is measured off of the delaminated face of the specimen where the end of the insert can be plainly seen. Measured load was then plotted versus displacement and a line was marked through the initial linear portion of the load curve. From the graph, the slope of the linear portion, the load were the loading curve deviated from linear, and the maximum load point were recorded. The load values of each test were corrected by the zero load point reading taken from the load cell just after each specimen broke. For the fastest tests a graph of load versus time was also plotted, and the slope of the initial linear portion was recorded as the loading rate. These measured parameters were used to calculate the toughness of each specimen using models presented in the analysis chapter and the results are presented in the results and discussion chapter.

CHAPTER IV

ANALYSIS

This chapter describes four types of models that were used in this dissertation research. The first section describes different compliance models. The second describes a viscoelastic fracture model that was developed to try to relate the time and temperature dependence observed in the strength data to that previously observed in compliance data. The third section describes a failure criterion based on the dilatational strain energy which is an alternative explanation to the fracture model. The fourth model development describes how the measured parameters of the DCB test are used to calculate fracture toughness.

Compliance Model

The model for the compliance of the matrix, D_m, is based on creep data for the K3B material. The data shown in Figure 11 was collected during a study on physical aging[21]. The curves in Figure 11 are momentary master curves, which means that each curve is the compilation of several tests conducted with different aging times. The data is then manipulated to form a curve for compliance at each temperature which is uniformly aged for 2 hr. Put another way, this data has been manipulated to remove the effects of aging that would ordinarily bias data from a creep test due to aging that occurs during a given test.

To convert this data into a viscoelastic compliance model that can be used at different temperatures, a master curve is formed from the data. Figure 12 shows that the data does form a well behaved master curve using a shift constant $\eta=29700°R$. The
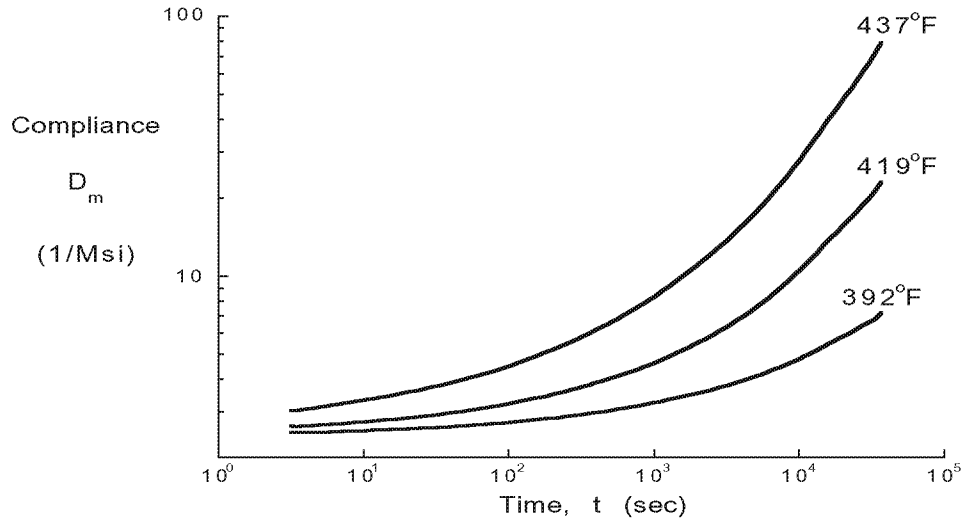
Figure 11. Compliance of K3B matrix[21].
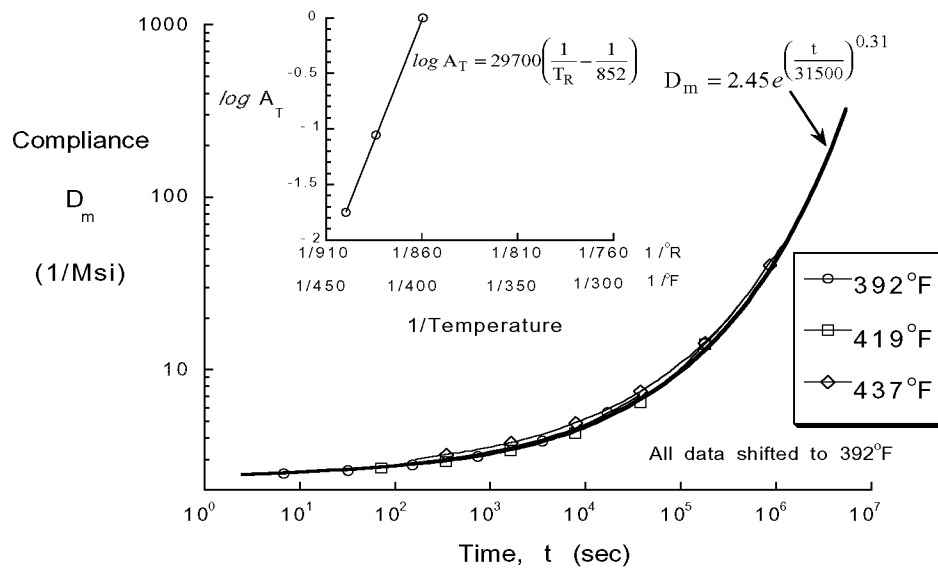
Figure 12. Time-temperature compliance master curve for K3B matrix.

44

master curve which was shifted to 392°F was fitted with a stretched exponential function which has the form

$$D_m = D_o \, e^{\left(\frac{t}{\tau}\right)^{\beta}}$$

(7)

where the initial compliance D_o has a value of 2.35 1/Msi, the time constant τ has a value of 31500 sec., and the stretch factor β has a value of 0.31. For the master curve to model compliance at other temperatures, it must be shifted in time using the shift constant used to form the master curve. The compliance model therefore becomes

$$D_m = D_o \, e^{\left(\frac{t}{\tau \, 10^{-29700\left(\frac{1}{T_R} - \frac{1}{852}\right)}}\right)^{\beta}}$$

(8)

One more correction needs to be made before this model can be used to predict the compliance of the matrix of the composite specimen used in this study. The momentary master curves presented in Figure 11 were for a uniform aging time of 2 hrs. To model the compliance of the material in this study which was aged for 66 hrs. at 400°F, the master curve must be shifted. From the same aging study[21], a shift rate μ for aging at 400°F was taken as 0.93. This shift rate was used in the following equation to obtain the appropriate shift to the master curve.

$$log(A_T) = \mu\left(log(t_{age}) - log(t_{ref})\right)$$

(9)

In the current case t_{ref} is 2 hrs. and t_{age} is 66 hrs. which gives a shift factor of 26.0. To shift the reference master curve, the shift factor is multiplied by the time constant τ. This produces a new master curve for the new aging time which is described by the same

45

stretched exponential equation but with a new time constant. In this case, the new τ is

820,000 sec. so the compliance model for the matrix becomes

$$D_m = 2.35\, e^{\left(\dfrac{t}{820,000\ 10^{-29700\left(\frac{1}{T_R}-\frac{1}{852}\right)}}\right)^{0.031}}$$ (10)

This visco elastic model for matrix compliance at various temperatures will be used in the following section as input into a fracture model for the composite.
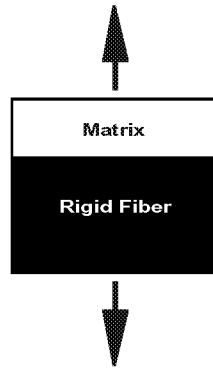
Figure 13. Diagram of a composite series model..

The viscoelastic matrix compliance model can also be used to predict the viscoelastic response of the composite. Of primary interest was the question, "How well can the nonlinearity in the transverse tension load strain response be explained by viscoelastic matrix model?" To answer this question the matrix compliance was related to the compliance of the composite through a simple series model. The series composite model is created assuming the matrix and the fiber materials are arranged in series as shown in Figure 13. Equation 11 relates the constituent properties to the composite properties for this type of composite model .

$$D_c = \upsilon_f D_f + \upsilon_m D_m$$ (11)

D and υ are respectively the compliance and volume fraction of the composite, fiber, and

matrix. For this type of graphite polymer composite where the matrix is much more

compliant than the fiber, the fiber can be assumed to be rigid ($D_f = 0$). Equation 11

therefore reduces to

$$D_c = \upsilon_m \, D_m \qquad (12)$$

This equation indicates that a simple scaling factor should be able to scale the matrix

compliance to that of the composite, and further that the scaling factor would have physical

significance as the matrix volume fraction.

Figure 14 shows how the K3B neat resin compliance was scaled to the composite

compliance for a transverse tension specimen tested at 300°F and 500 lb/sec. The

deformation response of this test was quite linear because of the high temperature and fast

loading rate. The figure shows that a scaling factor of 0.33 was need to scale the matrix

property to that of the composite. This factor is a reasonable value for matrix volume

fraction of this type of composite specimen.
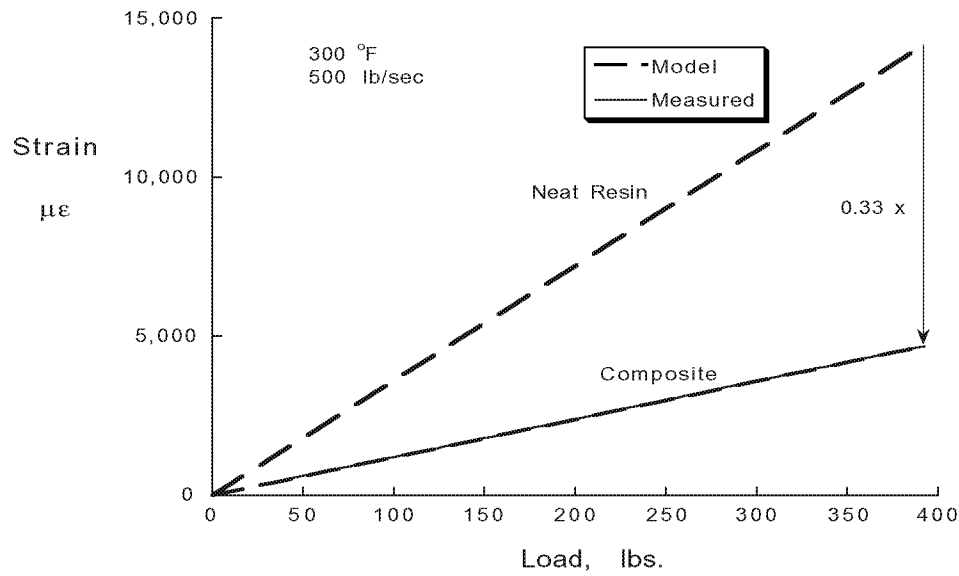
Figure 14. Scaling of matrix compliance.

This compliance model can now be used to predict compliance responses at test conditions where the material no longer behaves linearly. In order to calculate the viscoelastic deformation of the matrix or the composite from their respective compliance functions, a hereditary integral is used. The hereditary integral is presented in the background section as Equation 1 and is reprinted here.

$$\varepsilon(t) = \int_0^t D(t - \psi) \frac{d\sigma(\psi)}{d\psi} d\psi$$

D can be the compliance of the matrix or the composite depending on which material response is desired. Examples of predictions of viscoelastic deformation for the composite are shown in Figure 15 for constant ramp rate tests at 450°F which would be expected to show the most nonlinearity. The figure shows that the model predicts a significant difference in deformation response at the different loading rates and that at the slower

48

loading rates a large degree of nonlinear behavior is expected. The figure also shows the importance of accounting for the aging of the specimen with the unaged model showing significantly more deformation. These model predictions will be compared to the measured responses in the results chapter.

Viscoelastic Fracture Model

The viscoelastic fracture model developed here uses the matrix compliance data as input and calculates a fracture parameter which may be used to predict composite failure variation with time and temperature. This model is built on a crack tip energy fracture parameter described in the literature[44]. The W_f fracture parameter is physically the
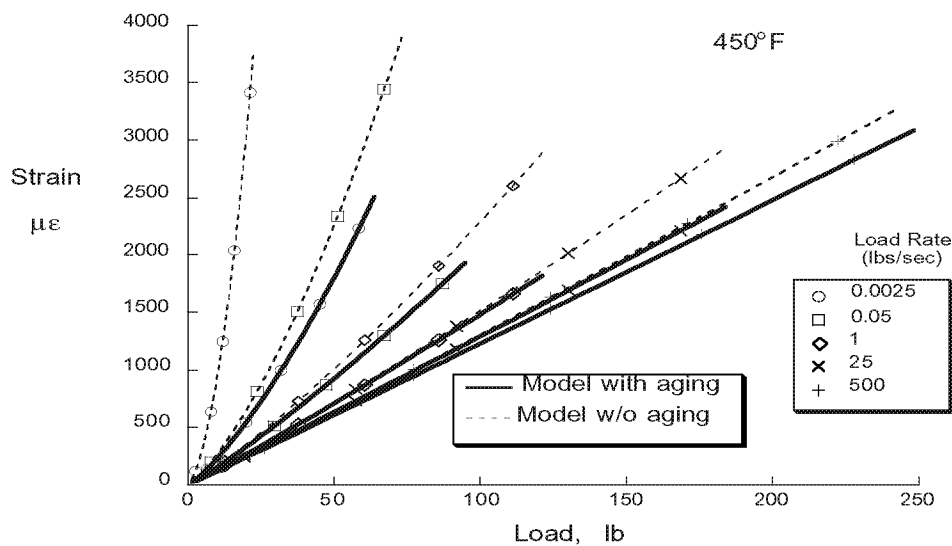
Figure 15. Composite compliance model predictions of deformation in constant ramp tests.

energy that is available to extend a crack tip and is defined in the following equation.

$$W_f = E \int_0^{t_i} D_m(t_i - \Psi) \frac{dJ^E}{d\Psi} d\Psi \tag{13}$$

J^E is the J integral of a body similar to the body of interest except that it is elastic with a

modulus of E. E is actually an arbitrary parameter which eventually cancels out of the

equation. D(t) is the compliance of the material in the process zone around the crack tip so

in this case it is the compliance of the matrix D_m and not the compliance of the composite.

W_f is calculated by this hereditary integral from 0, when loading of the body begins, to t_i

the time when the crack begins to grow. For an elastic body, compliance is not a function

of time so D can be removed from inside the integral which can then be reduced to J^E.

Since J^E is for the reference elastic system it is equivalent to G^E, the strain energy release

rate of the reference system. J^E is also related to K, the stress intensity factor through the

reference modulus and the Poisson's ratio ν. Of course the strain energy release rate is

only a function of the applied stress σ and the geometry factors such as crack size and the

specimen dimensions which are represented by the constant C_1.

$$J^E = G^E = \frac{1 - \nu^2}{E} K^2 = \frac{1 - \nu^2}{E} (C_1 \sigma)^2 \tag{14}$$

For the elastic case then Equation 14 reduces to

$$W_f = E D J^E = E D \frac{1 - \nu^2}{E} K^2 = (1 - \nu^2) D K^2 = G \tag{15}$$

Therefore in the elastic case, W_f is equivalent to the strain energy release rate.

The difference between W_f and G only shows up for an inelastic problem. G is

a measure of the energy that is supplied to a body from external sources and is a good

fracture parameter when one can assume that the energy that is supplied to a body is

readily available to extend the crack. For a viscoelastic body, this is not the case because, in

a viscoelastic body, the body itself absorbs energy like a sponge. It absorbs energy so that it is not readily available to the crack tip, and then at a later time, it may relinquish the energy making it available to the crack tip.

Failure in the viscoelastic model is assumed to be controlled only by the amount of energy that is actually available to the crack tip, thus W_f. Substituting the expression for J^E into the definition of W_f produces the equation

$$W_f = (1 - \nu)C_1^2 \int_0^{t_i} D_m(t_i - \Psi) \frac{d(\sigma^2)}{d\Psi} d\Psi \qquad (16)$$

Although it is not necessary that W_f be constant with time and temperature, if one does make that assumption, predictions of failure variation with time and temperature become very straightforward. One could test one specimen of a geometry where the strain energy release rate geometry constant C_1 is known. From Equation 16, the critical value of W_f could then be calculated using the time to failure and the other test parameters. The critical W_f could then be used to calculate the time to failure of any other loading history and geometry by inverting Equation 16. Of course the C_1 parameter would need to be known for the new geometry.

This model could also be used in cases where the geometry parameter is not known such as for transverse tension tests where crack growth from an initial flaw of unknown size and shape is assumed to control failure. One specimen of a given geometry would then be tested to failure. Lumping the W_f parameter together with the unknown geometry constants, a new constant could be defined that would be used as the critical parameter to predict the failure of the specimen subjected to different loading and temperature histories. This would not be as useful a result as the known geometry case because the results could not be translated to other geometries, but it would still be quite helpful because failure after

51

a wide range of loading and temperature histories could be predicted. To illustrate how this could work, the transverse tension tests conducted in this study will be used as an example.

The experiments in this study were performed with constant loading rates; therefore

$$\sigma \, w \, b = P = R \, t \tag{17}$$

where R is the loading rate and P is the applied load. When this expression is substituted into Equation 16, it produces

$$
W_f = (1 - v) C_1^2 \int_0^{t_i} D_m(t_i - \Psi) \frac{d\left(\left(\frac{R \, \psi}{w \, b}\right)^2\right)}{d\Psi} d\Psi \tag{18}
$$

$$
= \frac{2(1 - v) C_1^2 R^2}{w^2 b^2} \int_0^{t_i} \Psi \, D_m(t_i - \Psi) \, d\Psi
$$

By assuming that W_f is constant and collecting the terms that are constant for this experiment:

$$
R^2 \int_0^{t_i} \Psi \, D_m(t_i - \Psi) \, d\Psi = \frac{W_f \, w^2 \, b^2}{2(1 - v) C_1^2} = \text{Constant} \tag{19}
$$

The critical W_f is lumped with other constants to produce the constant C_2. Once the critical value of this constant is determined with one test, predictions of failure can be made for other temperature and load histories. Figure 16 shows predictions of this model created by inverting Equation 19 to predict times to failure at different loading rates and temperatures, assuming the compliance model developed in the previous section. Although the predictions in the figure are limited to simple constant load rate tests, it is not a necessary limitation. The Maple mathematical manipulation computer program [60] was used to create the contour plots in Figure 16 because inverting the integral in Equation 19 to obtain a function for t_i is not a simple operation. The data is presented as strength as a function of loading rate to emulate how experimental results might actually be presented.

Figure 16 shows that the model predicts strength decreasing with longer test times or slower ramp rates. One way of thinking about the results is to think of a failure occurring at a given stress level. If the time to reach that stress level were to be increased, the time for viscoelastic deformation would also be increased, therefore producing greater deformation. The model assumes that the work to failure is constant; therefore if the deformation increases, the critical stress would have to decrease since work is stress times deformation.

Without assuming that W_f remains constant with time and temperature, the predictive capabilities of the model become much more limited. Now instead of being able to predict a wide range of failure events with just one test, many would be needed. Once the failure contour for one specimen geometry is defined for how W_f changes with
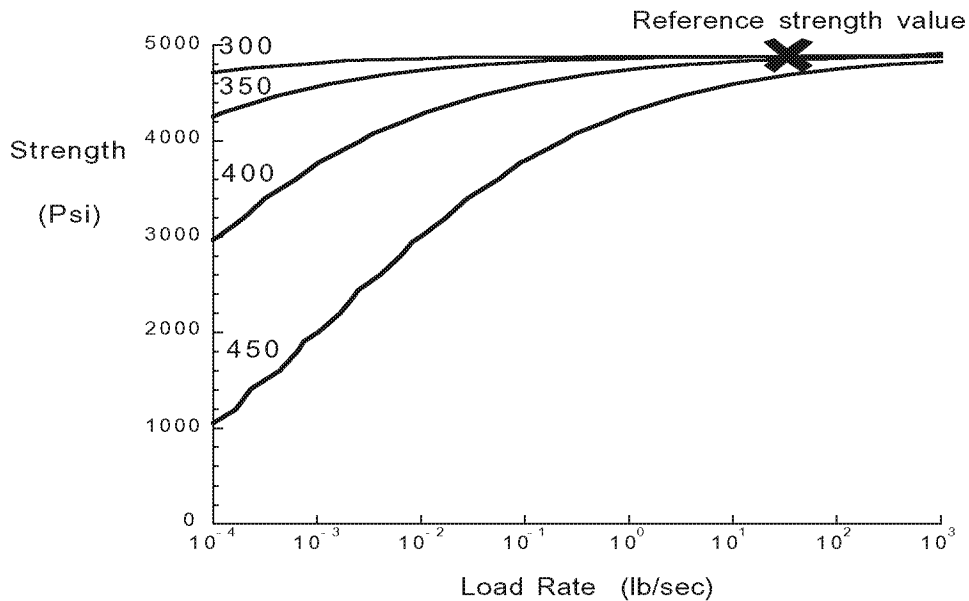
Figure 16. Constant W_f contours of strength predictions.

53

histories of load and temperature, it could then be used to predict the failure of other geometries. Defining the failure contour could be quite problematic however, since the variety of load and temperature histories to failure are unlimited.

Dilatational Strain Energy Model

The failure of composite material transverse to the fibers has been attributed to more than one failure mechanism. In the last section, a fracture model was presented which assumes failure occurs when the energy available to extend a crack from an inherent flaw reaches a critical value. A second failure criterion that has been studied assumes failure occurs when the dilatational strain energy density, $\mathcal{E}_{dil}$, at a point in the matrix reaches a critical value[30]. The dilatational strain energy is the energy stored by a material through volume expansion. Energy may also be stored in a material through shear, but it is assumed that this form of energy storage does not contribute to failure. The dilatational strain energy density is defined by the equation:

$$\mathcal{E}_{dil} = \int \left[\varepsilon_{xx} + \varepsilon_{yy} + \varepsilon_{zz} \right] d\left[\sigma_{xx} + \sigma_{yy} + \sigma_{zz} \right] \tag{20}$$

The σ and ε terms are the normal components of the stress and strain tensor, respectively.

The energy density will vary with position within the matrix because the stresses and strains vary.

To model the stress and strain variation within the composite, a micromechanics model is used. Figure 17 shows a diagram of the simple micromechanics model used along with the boundary conditions assumed. Note that the fiber is assumed rigid in this model and that the x and y axes are constrained by symmetry conditions. The top boundary is assumed to move up a constant amount V due to a force in the y direction and the shear stress on this boundary is assumed to be zero due to symmetry. The boundary conditions on the right side of the model are similar to the top conditions. No shear stress is allowed on the boundary and the lateral displacement is constrained to be constant. The only difference is that the force applied to the right hand side is constrained to be zero since no force is applied through the thickness of the laminate. The constraint in the fiber direction which is out of the paper for the micromechanics model is assumed to be plain strain.

P

$v(x,c) = V f_1(t)$ f_1 such that $\int_0^c \sigma_{xx}(x,c)\,dx = P$

$\sigma_{xy}(x,c)$

$u(0,y)=0$
$\sigma_{xy}(0,y)=0$

Viscoelastic matrix

Rigid Fiber

$u(x,y)=0$
$v(x,y)=0$

$u(c,y)=U f_2(t)$ f_2 such that $\int_0^c \sigma_{yy}(c,y)\,dx = 0$

$\sigma_{xy}(c,y)$

$v(0,y)=0$
$\sigma_{xy}(x,0)=0$
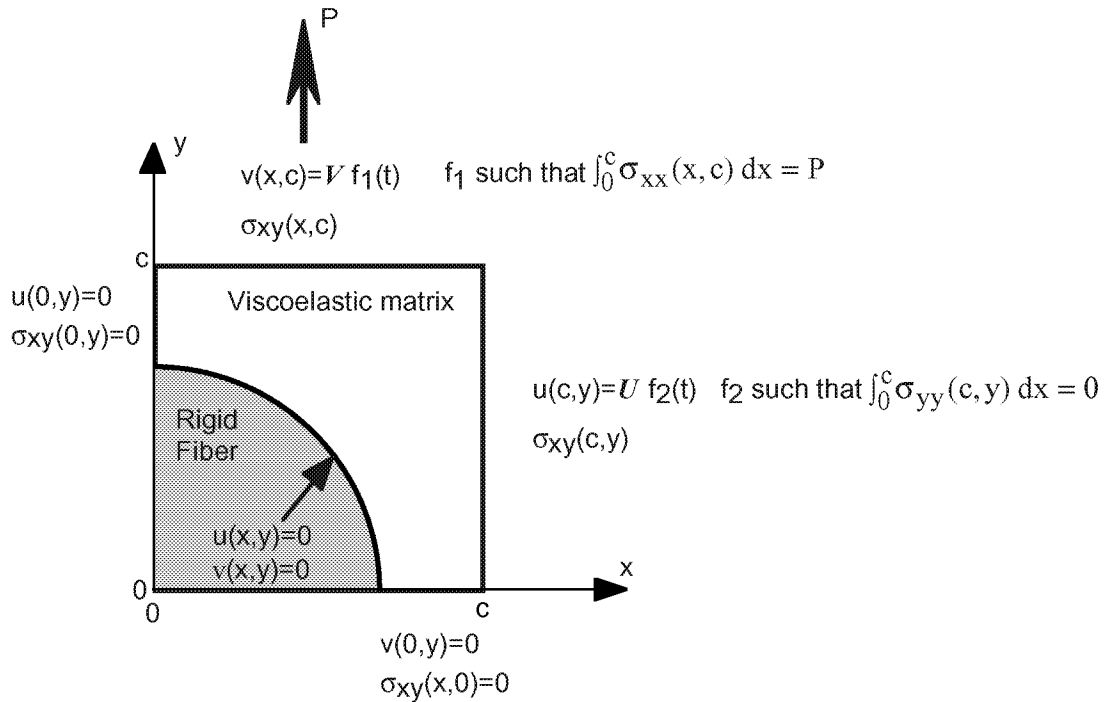
Figure 17. Micromechanics matrix model.

The boundary conditions on the micromechanics model allow the use of the Alfrey correspondence principle[61]. This principle assumes that the stress and strain solutions are separable in space and time as indicated in Equation 21.

$$\sigma_{ij} = \sigma_{ij}^{E} H(t) \quad \varepsilon_{ij} = \varepsilon_{ij}^{E} F(t)$$
$$u = u^{E} F(t) \qquad v = v^{E} F(t)$$

(21)

The spatial solution is given by an elastic solution to the problem designated by the variables with the superscript E because an elastic modulus, E, is assumed in the solution. The variation with time is described by the functions $F(t)$ and $H(t)$ which are chosen so that the boundary conditions can be satisfied and must relate to each other through the relation

$$F(t) = E \int_0^t D_m(t - \psi) \frac{dH(\psi)}{d\psi} d\psi$$

(22)

For the current problem which is loaded with a constant ramp rate

$$H(t) = P = R\,t$$
$$F(t) = f_1(t) = f_2(t)$$

(23)

In the application of the Alfrey correspondence principle, the assumption was made that the Poisson's ratio v does not vary with time. The constitutive equation for the matrix therefore is

$$\begin{bmatrix} \varepsilon_{xx} \\ \varepsilon_{yy} \\ \varepsilon_{xy} \end{bmatrix} = (1+v) \begin{bmatrix} 1-v & -v & 0 \\ -v & 1-v & 0 \\ 0 & 0 & 2 \end{bmatrix} \int_0^t D_m(t-\psi) \frac{d}{d\psi} \begin{bmatrix} \sigma_{xx}(\psi) \\ \sigma_{yy}(\psi) \\ \sigma_{xy}(\psi) \end{bmatrix} d\psi$$

$$\varepsilon_{zz} = 0 \qquad \left(\varepsilon_{xx} + \varepsilon_{yy}\right) = \frac{(1+v)(1-2v)}{v} \int_0^t D_m(t-\psi) \frac{d(\sigma_{zz}(\psi))}{d\psi} d\psi$$

(24)

Substituting Equation 24 into equation 20 and substituting Equation 21 and 23 produces

$$\mathcal{E}_{dil} = \mathcal{E}^{E}_{dil} \, E \int_{0}^{t} D_{m}(t - \psi) \frac{dP^{2}}{d\psi} d\psi$$

$$= \mathcal{E}^{E}_{dil} \, E \int_{0}^{t} D_{m}(t - \psi) \frac{d(R\psi)^{2}}{d\psi} d\psi \qquad (25)$$

$$= 2 \, \mathcal{E}^{E}_{dil} \, E \, R^{2} \int_{0}^{t} \psi D_{m}(t - \psi) d\psi$$

$\mathcal{E}^{E}_{dil}$ is the elastic dilatational strain energy density calculated from the corresponding

elastic problem. $\mathcal{E}_{dil}$ is a function of location only through $\mathcal{E}^{E}_{dil}$. It is assumed that failure

will occur when $\mathcal{E}_{dil}$ reaches some critical value, and it will occur at the location in the

matrix corresponding to the maximum in $\mathcal{E}^{E}_{dil}$. Equation 26 describes this failure

condition. The parameters which are constant in this study are collected on the right side

of the equation.

$$\left(\mathcal{E}_{dil}\right)_{crit} = 2 \left(\mathcal{E}^{E}_{dil}\right)^{max} E \, R^{2} \int_{0}^{t} \psi D_{m}(t - \psi) d\psi$$

$$R^{2} \int_{0}^{t} \psi D_{m}(t - \psi) d\psi = \frac{\left(\mathcal{E}_{dil}\right)_{crit}}{2 \left(\mathcal{E}^{E}_{dil}\right)^{max} E} = Constant \qquad (26)$$

The left hand side of Equation 26 is exactly the same as Equation 19 which was derived

from the fracture criterion. Therefore, the only difference in these failure criterion, for this

set of tests, is the interpretation of the physical constants. Therefore, strength predictions

from the dilatational strain energy model would look exactly the same as predictions from

the fracture model as long as the geometry remains constant. Assuming the critical

dilatational strain energy remains constant with time and temperature gives identical

predictions of strength to that presented in Figure 16 for the fracture model.

Although the predictions from the dilatational energy model are the same as the

fracture model, for a given geometry, the predictions of strength would change for different

types of specimen and might not be expected to model the failure of a fracture type specimen. This model will provide an alternative physical interpretation for the results presented in Chapter V.

Double Cantilever Beam Model

The double cantilever beam (DCB) test is a standardized fracture toughness test [62]. However to calculate a toughness value from the experimentally measured values a fracture model is needed. The standard defines the fracture toughness as

$$G_{Ic} = ERR = \frac{1}{w}\frac{dU}{da} = \frac{3P\delta}{2wa} \tag{27}$$

where the subscript Ic indicates a toughness value from a mode I test where the faces of a crack are pulled open as opposed sliding over each other. G_{Ic} is equal to ERR, the energy release rate, if the material is elastic. U is elastic strain energy, a is delamination length, and δ is the applied displacement. In the standard, three different methods of calculating the toughness parameter are presented which account for small variations of the specimen response from that predicted by simple beam theory. Each of these methods were based on a recorded history of load, displacement and delamination extension. In this study, it was not possible to record the delamination extension history of all the specimens so ERR was calculated more direct from the above definition. The slope of the initial linear portion of the loading curve is defined

$$m = \frac{P}{\delta} \tag{28}$$

substituting this into Equation 27 produces the equation

$$ERR = \frac{3P^2}{2wam} \tag{29}$$

This equation was used to calculate energy release rate values from the parameters measured during the DCB tests. Two values of critical applied load are suggested in the standard: the point of deviation from linearity and the maximum load point. These two points produce release rate values that may be seen as lower and upper bounds on elastic materials. The use of both critical points will be explored. The dimensions of the specimens were chosen using formulas given in the standard so that geometric nonlinearities should be insignificant.

Equation 29 calculates ERR assuming the material is linear elastic which would make it equal to G_{Ic}. The material in this study contains a matrix material that is viscoelastic in the time and temperature ranges tested. Goetz [63] showed that the deformation of this type of unidirectional DCB specimen is primarily controlled by the elastic fibers, and therefore it is believed that that this type of elastic analysis is sufficient to calculated ERR and therefore G_{Ic}. Although the stiffness of the test specimen is believed to be largely controlled by the fibers which are linear elastic, it is possible that some energy is absorbed away from the crack tip region due to the viscoelastic properties of the matrix. For this reason the crack tip energy parameter W_f was calculated from these tests as well. The following equation is derived starting with Equation 13 and substituting Equation 14 and 17.

$$
\begin{aligned}
W_f &= E \int_0^{t_i} D_m(t_i - \Psi) \frac{dJ^E}{d\Psi} d\Psi \\
&= E \int_0^{t_i} D_m(t_i - \Psi) \frac{d \frac{1-\nu^2}{E}(C_2 P)^2}{d\Psi} d\Psi \\
&= E \frac{1-\nu^2}{E} C_2^2 \int_0^{t_i} D_m(t_i - \Psi) \frac{d(R\Psi)^2}{d\Psi} d\Psi \\
&= 2(1-\nu^2) C_2^2 R^2 \int_0^{t_i} D_m(t_i - \Psi) \frac{d\Psi^2}{d\Psi} d\Psi
\end{aligned}
\tag{30}
$$

Since W_f is equivalent to G for a linear material and the calculation of the G parameter in Equation 29 involved the initial slope of the loading curve, G is equivalent to W_f calculated using the initial matrix compliance D_o instead of D(t). The following equations result from this realization.

$$\frac{W_f}{G} = \frac{2\left(1-v^2\right)C_2^2 R^2 \int_0^{t_i} D_m(t_i - \Psi)\frac{d\Psi^2}{d\Psi}d\Psi}{2\left(1-v^2\right)C_2^2 R^2 \int_0^{t_i} D_o \frac{d\Psi^2}{d\Psi}d\Psi} = \frac{2\int_0^{t_i} D_m(t_i - \Psi)\frac{d\Psi^2}{d\Psi}}{D_o t_i^2}d\Psi \quad (31)$$

$$W_f = G_{Ic}\left[\frac{2}{t_i^2}\int_0^{t_i}\Psi e^{\left(\frac{t_i-\Psi}{820,000\;10^{-29700\left(\frac{1}{T-392}\right)}}\right)^{0.031}}d\Psi\right] \quad (32)$$

Equation 32 will be used to calculate the crack tip energy from the fracture toughness which will be calculated from the experimental results.

CHAPTER V

RESULTS AND DISCUSSION

This chapter describes the results of this experimental investigation, and discusses the ramifications of these results. The transverse tension test results are presented in the first section. The results are shifted in time to form a master curve and are compared to the predictions of the fracture mechanics model. To validate the compliance parameters which were input into the fracture model, compliance predictions are compared to the load displacement curves recorded during the strength tests. In the second section, the results of the double cantilever beam (DCB) tests are presented and shifted in time like the strength data. Because the analysis of the DCB tests depended on when during the test the delamination began to grow, a study of delamination growth is presented based on recorded crack growth images. The fracture results are again compared to the fracture model and followed by a discussion of the results.

Transverse Strength Tests

Strength tests were performed at four different temperatures and over five decades of time scale as described in Chapter III. The results of these tests are plotted in Figure 18. There is a large amount of scatter in the data which blurs the effect of loading rate and temperature, but scatter is a common problem for this type of transverse tension specimen. The scatter is believed to be due to the premature failure of some of the specimen. The strength of a test specimen may be artificially low for many reasons: specimen misalignment, damage caused during specimen machining, stress concentration due to griping, etc. Because there are many reasons that would cause a specimen to be abnormally low but next to none that would cause a specimen to show an artificially high strength, only the highest three strength values at each test condition were used in the rest of this study. The strength results are replotted in Figure 19 with the lower strength values

61
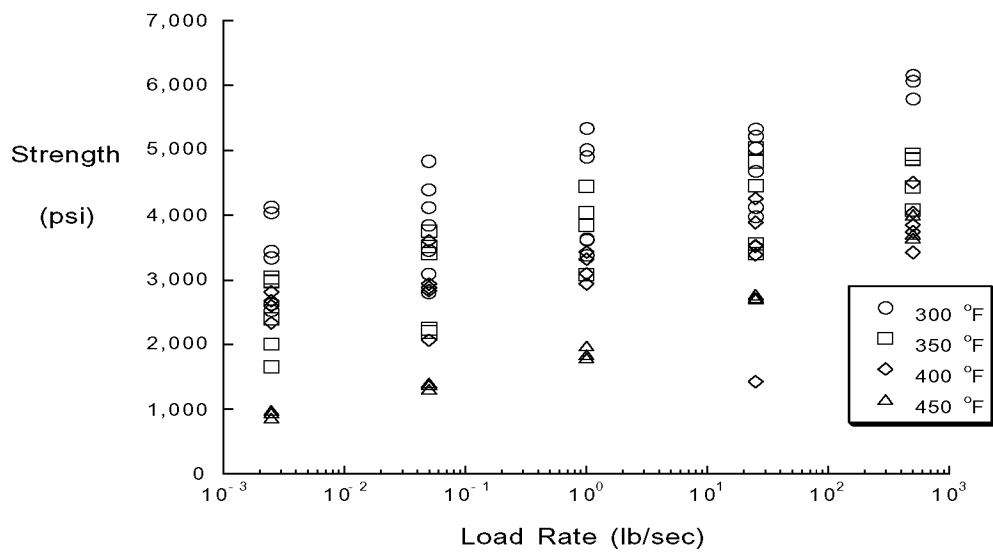
Figure 18. Results of transverse tension tests on K3B/IM7.
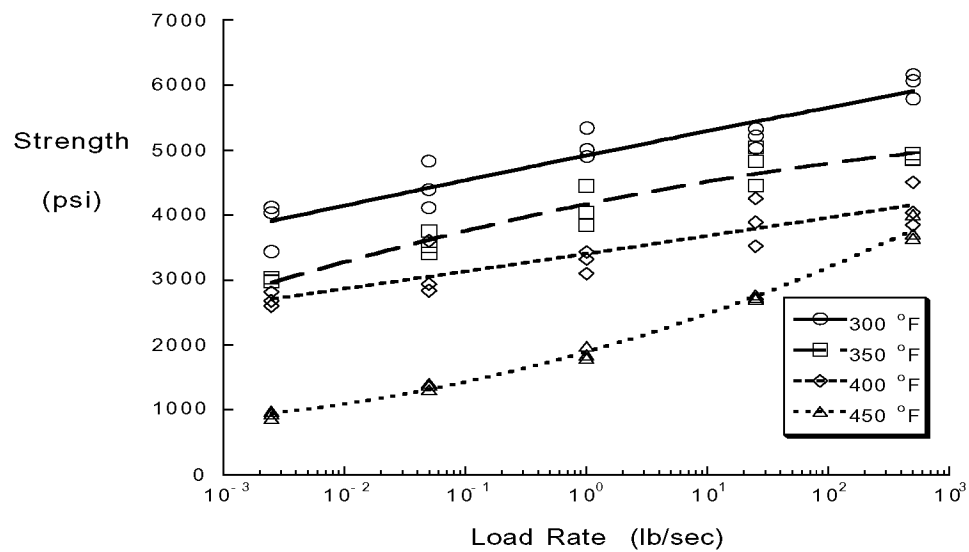
Figure 19. Filtered IM7/K3B transverse strength results (highest three strengths at each condition).

filtered out. It is obvious that not only is the scatter greatly reduced, but trends in the data

can be much more readily seen. Some of the strength results that were filter out, showed

edge defects or failures at the grip line, but not all the rejected data showed signs of

problems. Of the data that was kept some failed at the grip line which can be a sign of early

failure due to stress concentrations but can also naturally occur due to random strength

variations along the length of the specimen. On Figure 19, the trends in the data are marked

by second order polynomial curves fitted through the data by a least squares procedure. At

each temperature tested, the strength decreases by at least 25% over the 5 decades of time

scale tested. At 450°F, which was the temperature at which the strength was the most

sensitive to loading rate, the strength dropped by 66%. The highest strength was always at

the highest loading rate and therefore the shortest test. The numerical strength data are

listed in Table 1 of the Appendix.

The strength results also show a significant temperature dependence. Each
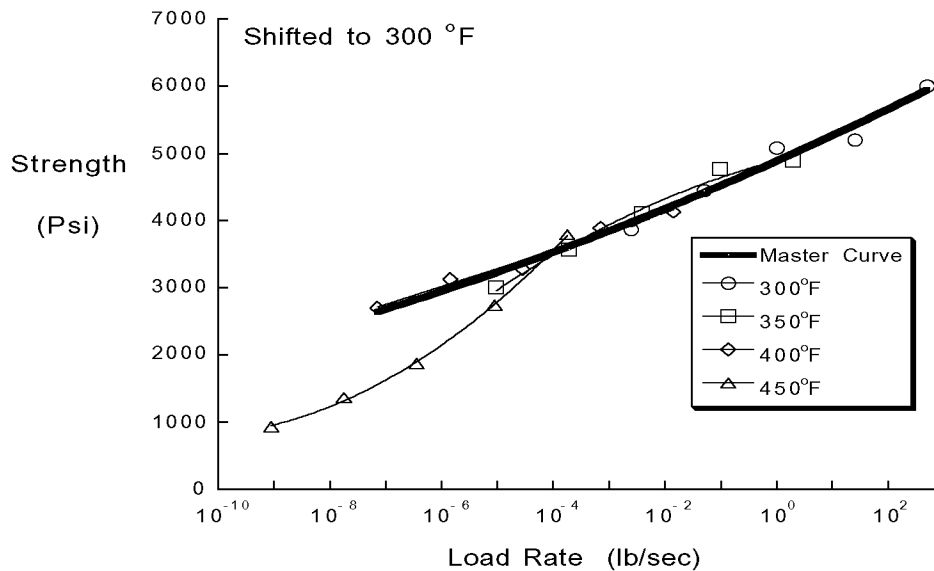
Figure 20. Transverse tension strength results shifted to 300°F.

increment of 50°F reduced the strength at a given loading rate by an average of 900 psi. The curves also lie approximately parallel to each other in a manner which might allow them to form a master curve, except for the results at 450°F. Figure 20 was created by shifting the results presented in Figure 19 using the same shift constant (η=29700 °R) that created the matrix compliance master curve shown in Figure 12. On Figure 20, the filtered data is shifted to 300°F, and only the averages of the replicate tests are shown. The light lines are the best fit lines from the previous figure shifted in time. The strength results up to 400°F do appear to form a fairly well behaved master curve as shown by the heavy line. At 450°F, the strength has dropped off faster than would have been predicted by the master curve fitted through the remaining data.

The formation of the master curve indicates that an increase in temperature creates an effect that is comparable to increasing the time scale. The formation of a master curve allows the prediction of the 300°F strength tested at a loading rate of 10^{-7} lb/sec which would require approximately 50 years to conduct. If the 450°F data had also fallen on the master curve, 300°F tests conducted at 10^{-9} lb/sec could have been predicted which would have required 5000 years to conduct. The current master curve allows predictions of 350°F tests lasting half a year while 50 year tests could have been predicted if the 450°F tests had also fallen along the master curve.

Although this way of making predictions of strength over long time scales is significant, the technique is only good for accelerating similar load histories at a constant temperature. These results could not be used to predict a creep test where the load is held constant until specimen failure. These results would also prove insufficient for predicting constant ramp tests during which the temperature changed. For these results to be used to predict failures based on different load and temperature histories, the cause of failure including the effect of time and temperature must be understood. Because the shift constant for strength is the same as the shift constant for modulus it is suspected that the two time dependent effects may be due to the same phenomenon. The change in strength with time

may even be caused directly by the change in modulus. One model that would relate compliance to strength is the fracture mechanics model presented in Chapter IV.

The fracture mechanics model assumes that the strength of the composite is actually controlled by a fracture phenomenon. The composite therefore breaks when the energy level in the composite reaches a level where a crack is able to grow from an existing flaw. The fracture model uses the compliance of the matrix and the load history to calculate an energy parameter W_f. W_f is the energy that is available to extend the crack tip of an existing flaw. When the critical value of W_f is not known, one strength test can be used to back calculate W_f and then assuming that W_f remains constant, predictions can be made of strength at other times and temperatures. Figure 21 shows the experimental results presented in Figure 20 with the constant W_f model fitted to two different strength values. It is clear from the graph that this simple fracture model is not capturing the material behavior,
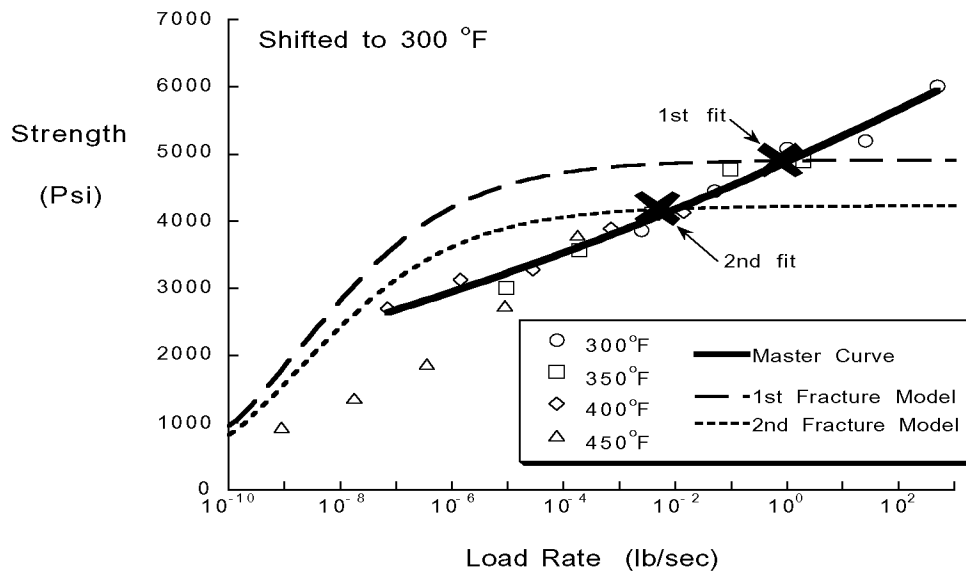
Figure 21. Fracture model fitted to strength results time shifted to 300°F.

and that using a different constant value of W_f would not help significantly.

One possible problem with the model is that the neat resin properties that are used as input to the model may be significantly different from the properties of the matrix material which is in the composite. To test for this difference, the load-strain results from the composite compliance model were compared to that of the measured response from the strength specimen. Figure 22 shows these results for the slowest ramp rate at each temperature. The model seems to predict the experimental results quit well at 400°F and below, but at 450°F, the measured compliance is much greater than predicted. This is an indication that at 450°F the temperature is getting so close to the glass transition temperature that the material properties are beginning to change very quickly. This would also be a reason why the 450°F strength data does not fall on the master curve created by the strength values at the lower temperatures.

Figure 23 shows the composite compliance model prediction for the 400°F tests at
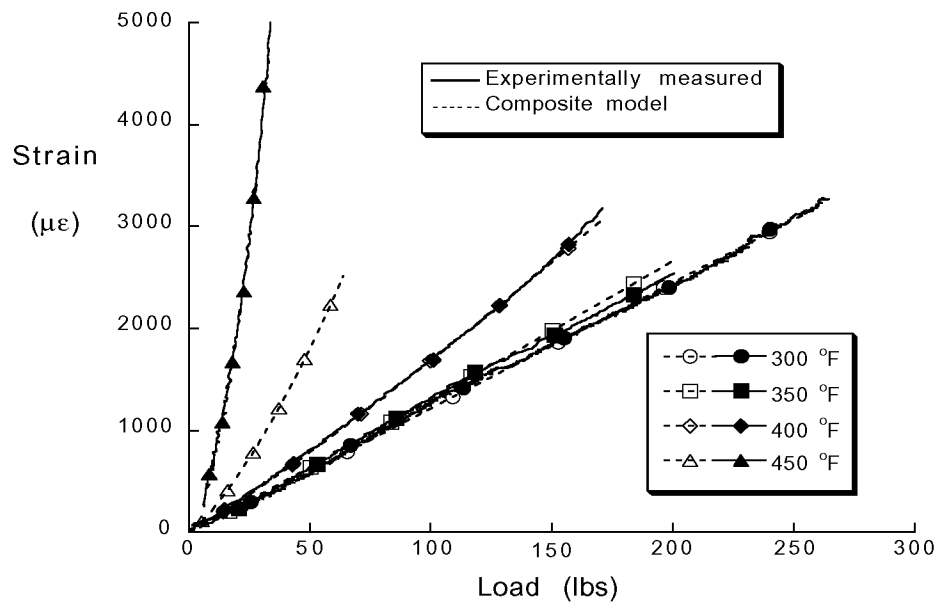
Figure 22. Strain response of slow ramp tests (0.0025 lb/sec).

all the different loading rates tested. The agreement between the predictions and the measured response indicates that the model is doing a good job of capturing the time-dependent deformation at this temperature. This can be compared to the comparable results at 450°F which are shown in Figure 24. At 450°F, the measured strain is significantly higher than the predictions at each of the loading rates. The compliance model of the composite, and therefore of the matrix, seems to be doing an adequate job below 450°F so this should not be the reason for the poor agreement between the fracture model and the experimentally measured master curve.
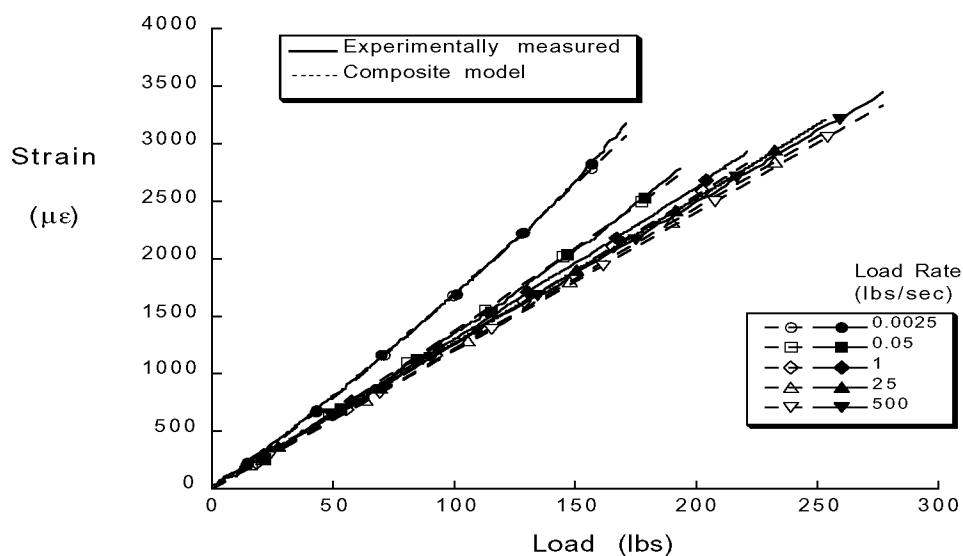
Figure 23. Strain response at 400°F.
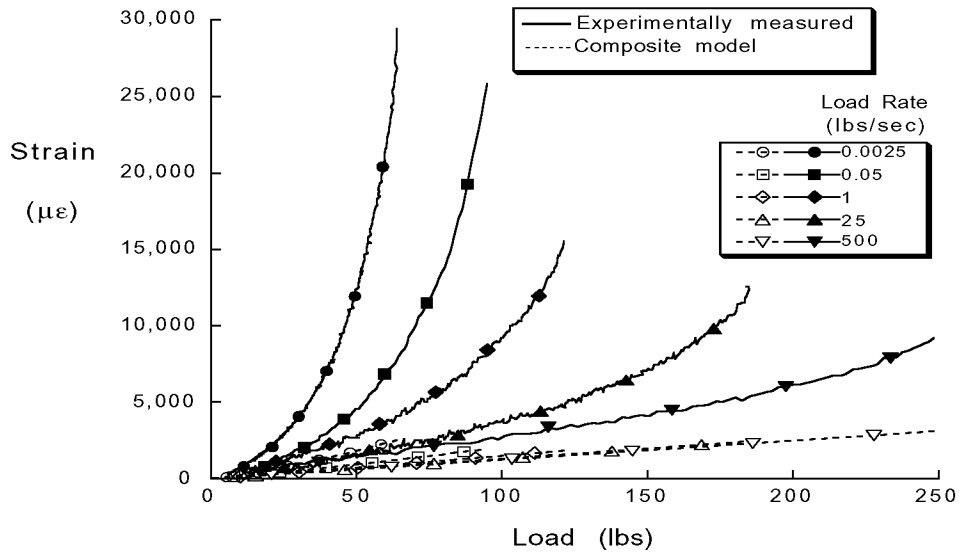
Figure 24. Strain response at 450°F.

The fracture model predictions shown in Figure 21 are based on the assumption that the W_f parameter is not a function of time and temperature. Although there is a significant modeling advantage should W_f remain constant, there is no reason that it must. Assuming that all the tension specimens are of similar geometry, the variation of the W_f parameter among the different tests can be calculated as shown in Figure 25. Because the geometry constant that relates the stress to W_f is not known, the absolute magnitude of W_f cannot be determined. Since only the relative magnitude of the W_f is known for the different test conditions, it is plotted in Figure 25 normalized to the highest value. It is obvious from the figure that the fracture parameter does change significantly with ramp rate, but at least it is fairly well behaved. On this plot where the data has been shifted using the compliance shift factors, all data falls on a master curve except for the 450°F data. Fitting a line through the remaining data on this log-log plot produces a expression for the W_f master curve. At 450°F, the W_f values are questionable because the compliance model used to calculate W_f greatly underestimated the actual deformation of the material. If the material compliance

68
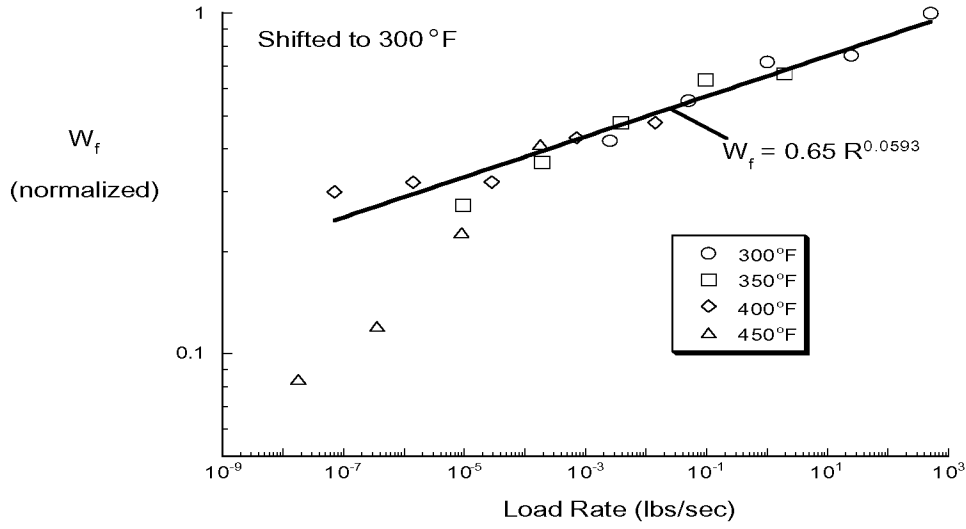
Figure 25. W_f results from strength tests.

were correctly modeled at 450°F, it is possible that these W_f values would be high enough to also fall on the master curve.

The fact that W_f appears to be a function of rate may not be a complete surprise if one considers the Dugdale assumption [64] that

$$G_{Ic} \cong \sigma_F \, \delta_{CTOD} \tag{33}$$

σ_F is the flow stress for the material at the crack tip which might be assumed to increase with increasing load rates. δ_{CTOD} is the critical displacement at the crack tip which has been shown to remain constant over a range of temperatures for certain classes of materials [65] and therefore might be expected to be constant with time as well. Therefore a rate dependence of σ_F would produce a rate dependence in G_{Ic} and therefore in W_f which might explain the rate dependence seen in Figure 25.

69

Using the expression for how W_f changes with rate, predictions can be made with the fracture model. Figure 26 shows that the variable W_f model does a very good job of modeling the experimental results below 450°F. At 450°F, the model does not do such a good job. The fact that the model fits the data well below 450°F should not be a surprise since the curve was in fact fitted to the data, just in a transformed space.

If W_f is shown to be the controlling parameter for these failures, then this model will allow these results to be used to predict failures of other geometries where fracture is the controlling mechanism. Unfortunately because W_f is changing, predictions of tests with other types of load-temperature histories could not be predicted without further understanding of how the W_f parameter changes with changing load and temperature histories.

To test the hypothesis that W_f is the controlling parameter in these tests, constant load rate tests of a common fracture test were performed.
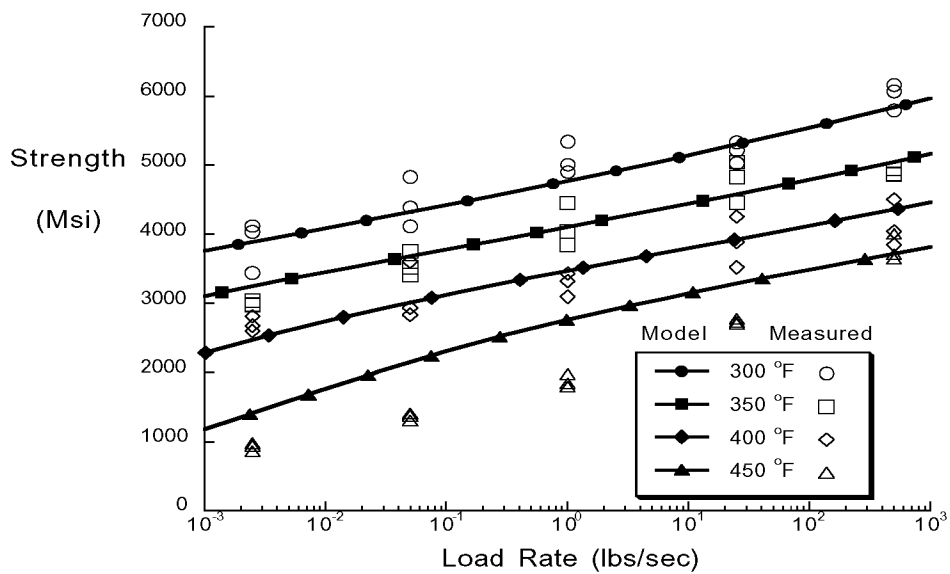
Figure 26. Strength predictions assuming varying W_f.

70

Double Cantilever Beam Tests

DCB tests were performed at three different temperatures and over five decades of time scale as described in Chapter III. A typical load history from one of these test is shown in Figure 27. From this test at 400°F and 0.006 lb/sec, it is clear that a significant amount of nonlinearity occurs in the load displacement curve before the maximum load is reached. This could be due to material nonlinearity, or it may be due to delamination growth. The amount of nonlinearity is more than might be expected from the matrix compliance response shown in Figure 11. Delamination growth is also somewhat unexpected because the test is conducted with a constant loading rate rather than the usual constant displacement rate. With this type of test, one would expect the delamination to grow to failure as soon as it begins to grow, because the strain energy release rate will increase with delamination length. A delamination can grow stably in spite of the increasing strain energy release rate, if the materials exhibits a steep R-curve effect, which is to say that the material's resistance to delamination increases quickly as the delamination grows. Since the W_f model is an initiation model, it is important that the critical point where the delamination begins to grow be determined.

Two points were recorded from each test, the point where the maximum load is

reached and the point where the loading curve first deviates from linear. These points are

shown on Figure 27. The nonlinear point is more subjective than the maximum load point

because the deviation from linear is usually subtle. To help identify the nonlinear point, a

line is marked through the linear portion as shown in Figure 27. The placement of the line

is also somewhat subjective because of the small amount of drift in the load signal. The

small amount of drift in the load signal can mask the small deviation from the linear load

path. Acknowledging these difficulties, efforts were made to be as consistent as possible in

determining the nonlinear load point. The value of the critical load points from each test are

shown in Figure 28. The numerical data for these toughness tests are listed in Table 2 of

the Appendix. There is significantly less scatter in the maximum load data than in the point

of nonlinear deformation, possibly due to the greater subjectivity required in determining the
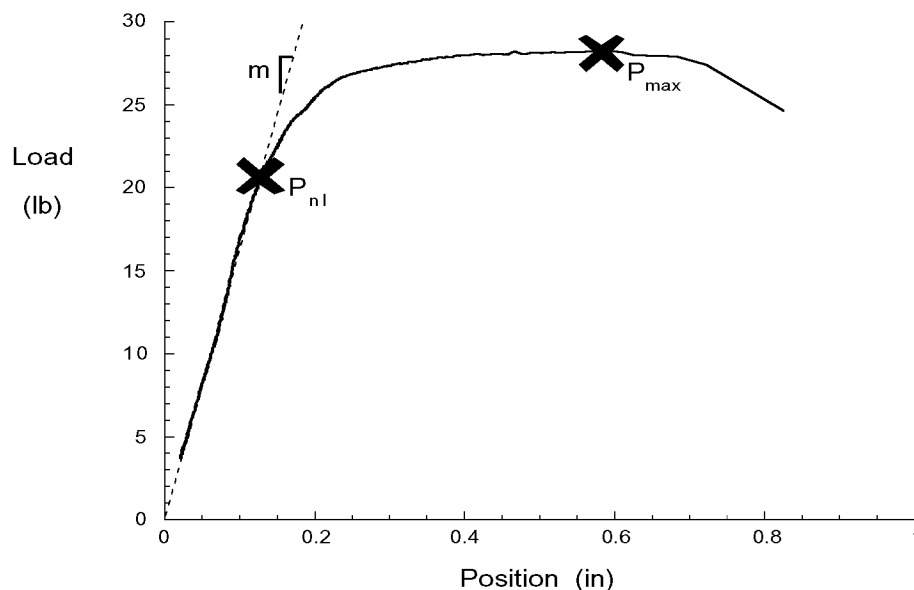
Figure 27. Typical load-displacement response from DCB test.
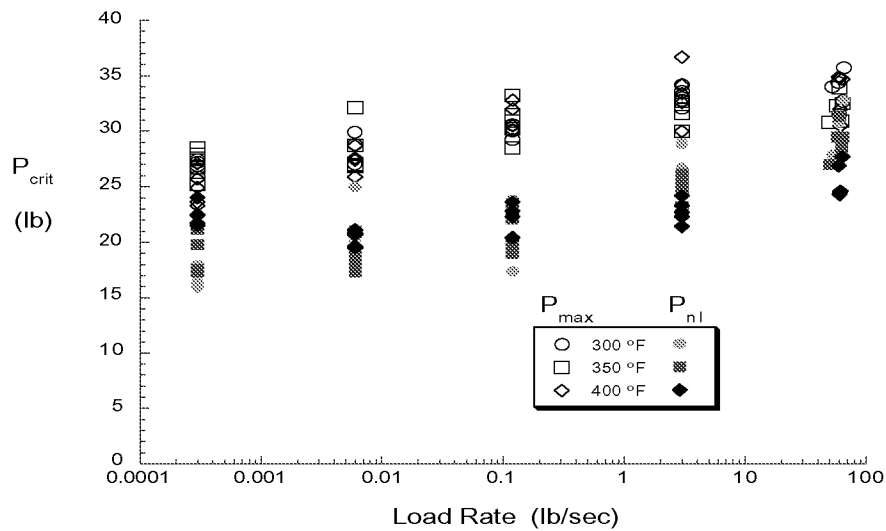
Figure 28. Critical load data from DCB tests.

nonlinear point. Both sets of data show a significant variation with loading rate but appear to have only a slight dependence on temperature.

To determine whether the maximum load point (P_{max}) or the nonlinear load point (P_{nl}) is the appropriate critical point, a few of the test were observed with the long focal length microscope described in Chapter III. Video images of the delamination tip were recorded during a test. When the delamination grew, the microscope panned to follow the crack tip. After the test, the video images were translated into computer images and made into a mosaic as shown in Figure 29. The time at which each image on the mosaic was recorded was noted and surface features were used to position the images so that they had a constant horizontal reference point. This was necessary because the camera followed the delamination tip. Once the mosaic of the video images was created, a record of

73
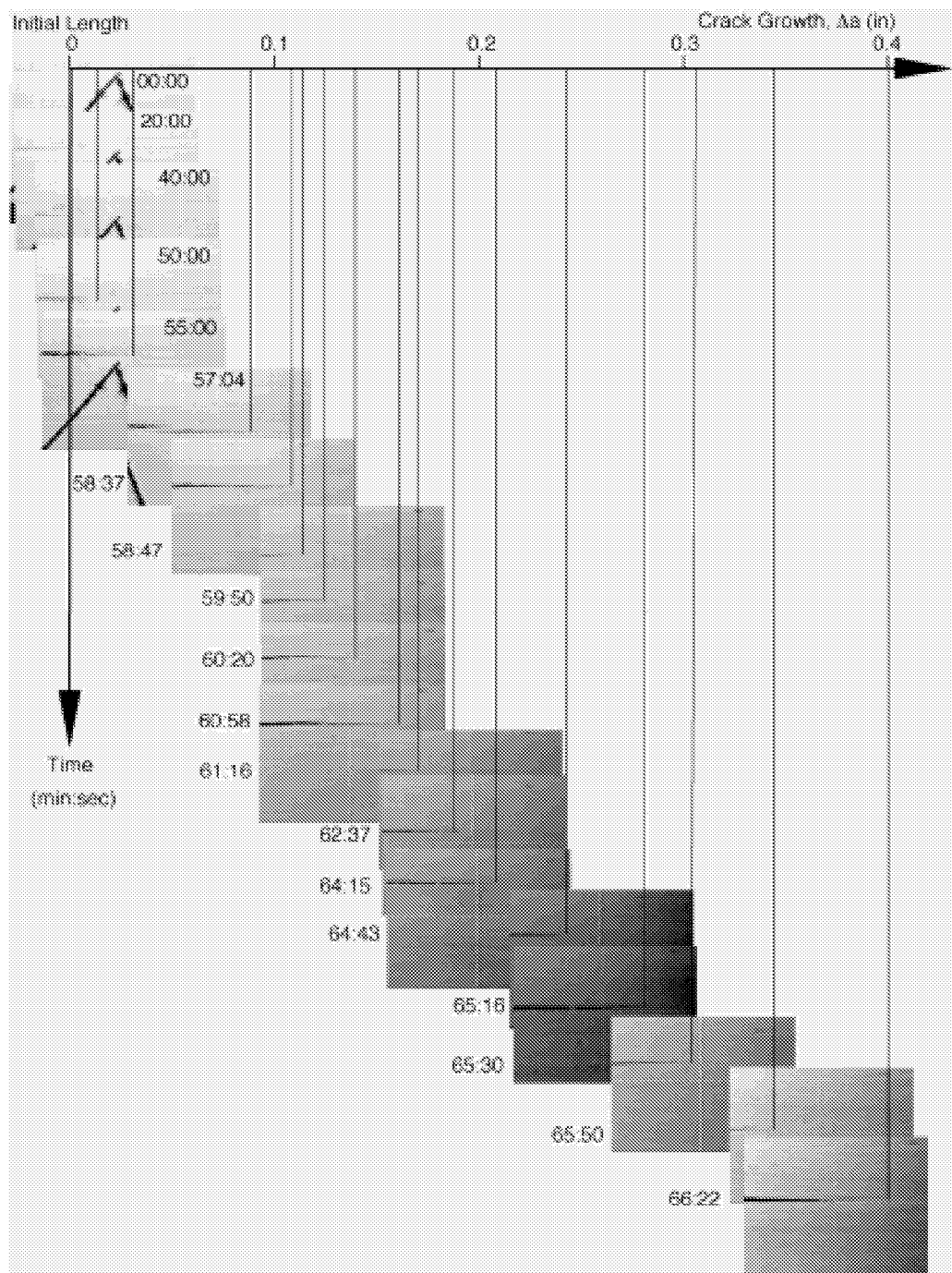
Figure 29. Mosaic of delamination growth images.

delamination growth could be made. Figure 30 shows the record of delamination growth

and compares it to the position time history for the test. Because the test was run with a

constant loading rate, the time scale is also an indicator of load so the nonlinear and

maximum points correspond to P_{max} and P_{nl}. Notice that the first observation of

delamination growth occurs just after the nonlinear point on the delamination curve. The

maximum load point occurs after substantial delamination growth and after the crack

growth rate is too fast to be followed by the camera.
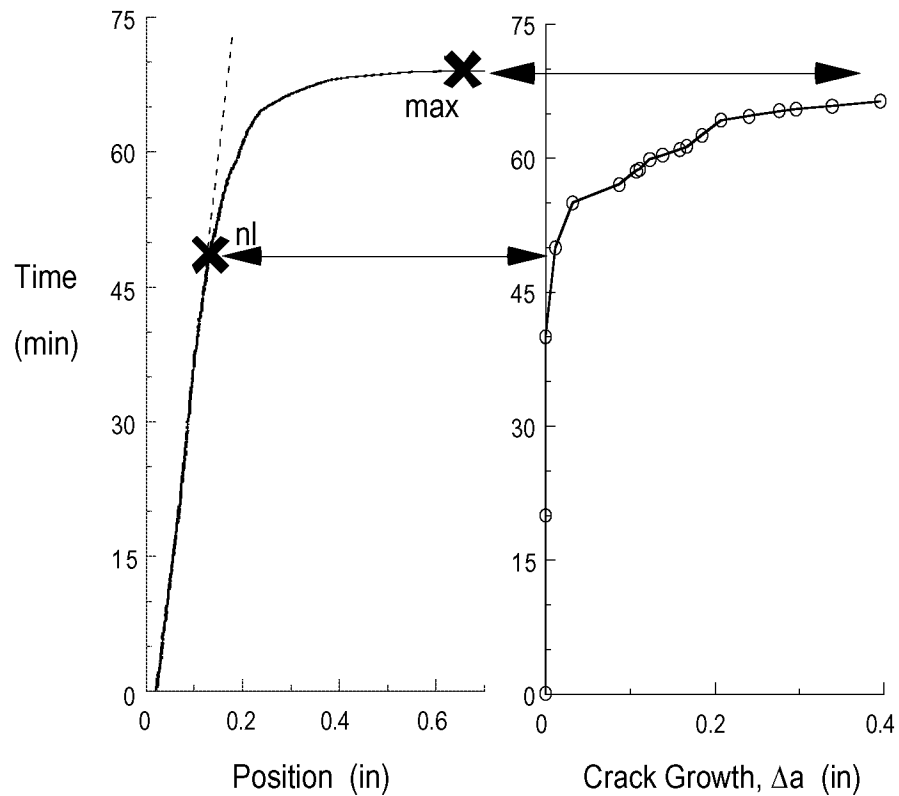
Figure 30. Displacement history compared to delamination growth.
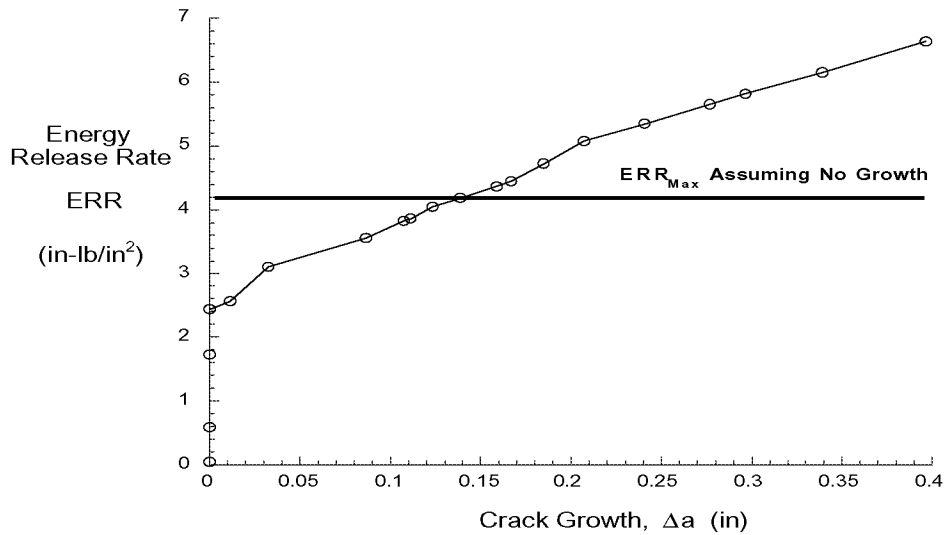
Figure 31. R curve from a DCB test.

The record of load, displacement, and crack growth was used to create the critical

energy release rate values shown in Figure 31. These energy release rate values are equal

the fracture toughness G_{Ic} if the crack extension is the only energy absorbing mechanism in

the specimen. As discussed in the DCB analysis section, this is believed to be a good

assumption for this type of unidirectional DCB specimen. This type of graph that shows

how fracture toughness changes with crack advance is called an R curve. This R curve is

quit steep, with the toughness nearly tripling as the delamination advances by less than a

half an inch. It is this steep R curve that allows the delamination to grow in a stable manner,

even in this type of constant load rate test. Unfortunately this increase in fracture toughness

is believed to be due to fiber bridging[66-68], which is an artifact of this type of

unidirectional test specimen and does not correspond to an increase toughness seen in real

structures where delaminations grow between layers of different orientation. From these

crack growth results, it is clear that the nonlinear point is the critical point that should be

76

used to calculate the initiation ERR. Plotted on Figure 31 is also the initiation ERR value that would have been calculated if the maximum load point were used along with the initial delamination length. This mistake would have produced an apparent initiation value that was 1.7 times the actual value.

The nonlinear load point was used to calculate the initiation energy release rate values for each specimen tested at the different temperatures and loading rates. The results are shown in Figure 32. Five specimen are tested at each condition, and the data at each temperature is fitted with an exponential equation that produces a linear fit on this log-log plot. Again assuming that the energy release rate values correspond to the toughness of the material for this type of specimen, the results show that delamination toughness is significantly affected by loading rate. The initiation toughness varies by nearly 3X at 300°F but only 1.3X at 400°F. The values of the exponential terms of the least squares fits to the data in Figure 32 bound the 0.059 value determined from the W_f data plotted on Figure 25. At the slower loading rates, there seems to be a reversal of the trend for increasing
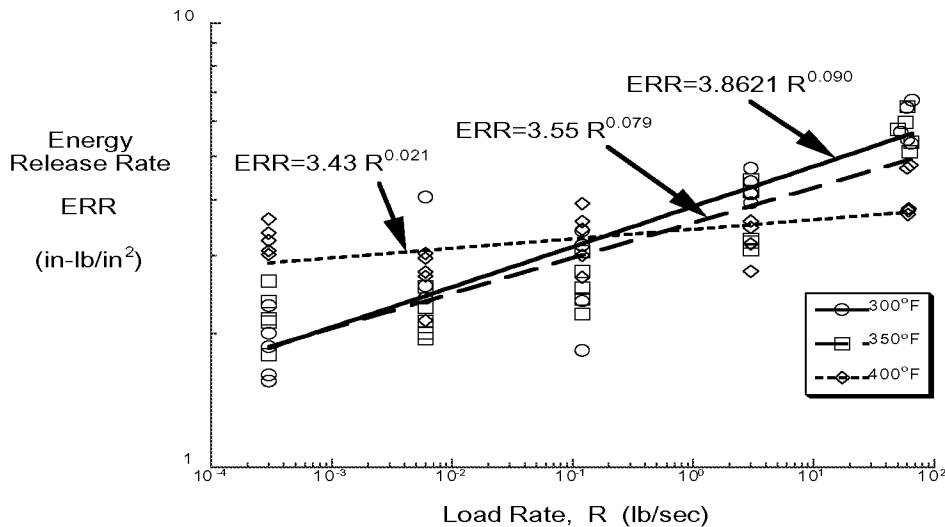
Figure 32. Delamination energy release rate results.

temperatures to decrease toughness. One explanation for this can be postulated by again relying on the Dugdale assumption described earlier by Equation 33. Kinloch and Young [65] showed that over a large range of temperatures δ_{CTOD} remained constant, but they also showed that at higher temperatures, which might also correspond to slower load rates, δ_{CTOD} can increase quickly. The increasing toughness with increasing temperature at low load rates could therefore be due to an increase in the δ_{CTOD} under these conditions. The δ_{CTOD} would need to increase faster than the σ_F decreases to explain these results.

The correspondence between temperature and loading rate is also complicated. The curves at different temperatures do not parallel each other in a way that would easily form some type of master curve. The data is shifted with the shift rates developed for compliance in Figure 33. On the figure, the average of the five replicate tests at each test condition is plotted along with error bars showing one standard deviation above and below the mean.
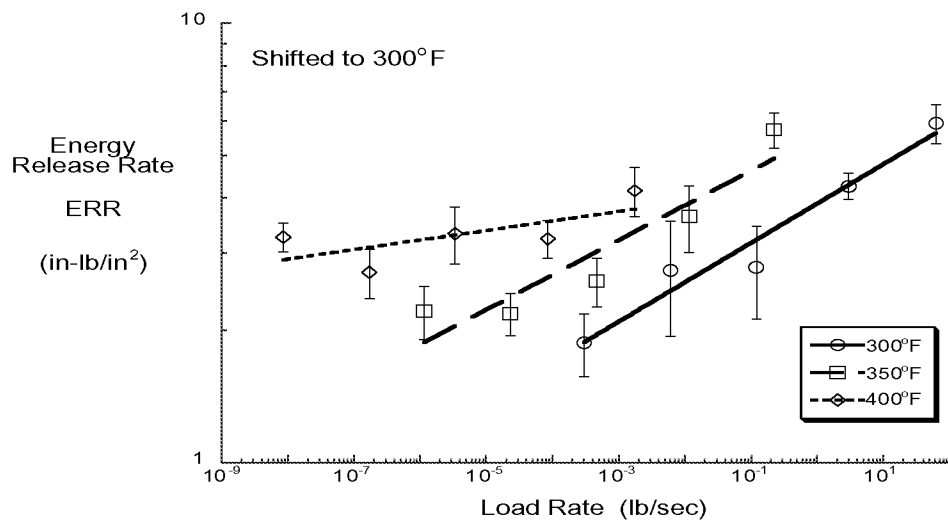
Figure 33. Shifted energy release rate results.

The curves at different temperatures do not fall near each other in a way that would suggest a master curve. In fact, the data came closer to forming a master curve before the time shift was made.

Although the loading to the point of delamination growth appeared quite linear, the neat resin compliance results would suggest that there is some degree of viscoelastic material response occurring during the DCB tests at the temperatures and loading rates tested. To account for viscoelastic deformation that may occur in the matrix away from the crack tip region, W_f values are is calculated from the experimentally measured values using Equation 32 from the analysis chapter, and the results are plotted in Figure 34. The results at different temperatures have been time shifted in this figure as they had been in Figure 33. Notice that except for at 400°F, the difference is quite small between W_f and G_{Ic}, which is assumed to be equal to ERR. At 400°F, the difference becomes larger as the loading rate is reduced. From the W_f results, it is clear that this attempt to include the effect of viscoelastic
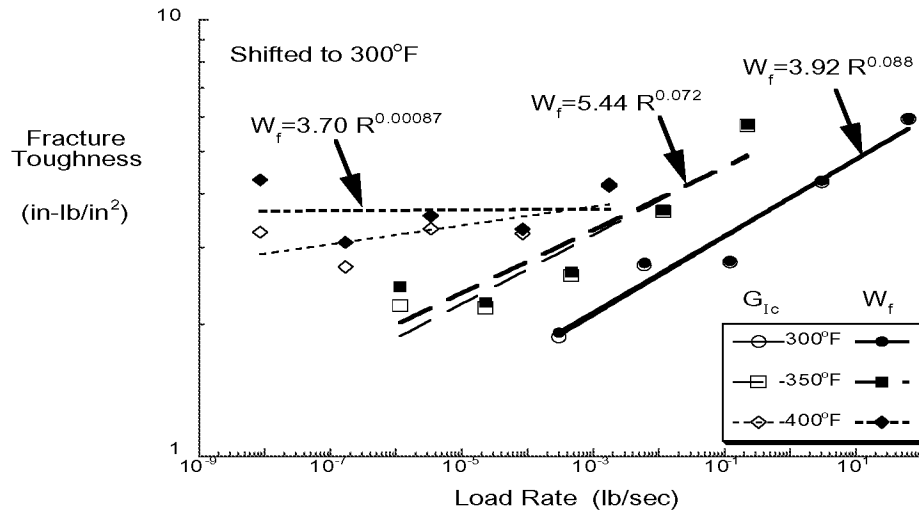
Figure 34. Comparison between G_{Ic} and W_f results shifted in time.

deformation of the matrix away from the crack tip does not help form a master curve from the toughness data. Because of the linear loading curves, it is believed that the simple G analysis is appropriate to analyze the test results. The W_f parameter for the DCB test, would have been more appropriate if a viscoelastic response had shown up in the loading curve as a nonlinearity prior to delamination growth.

Because the toughness response of this DCB fracture test does not form a master curve as the strength data did, it seems that the fracture model may not be an appropriate model to explain the strength results. The DCB results do indicate that the interlaminar fracture of this composite material is complex. The W_f model is a fairly simple fracture model which assumed such things as a linear viscoelastic material response. The W_f model is also an initiation criterion and was applied to the strength data assuming that once a crack grows from an initial flaw, it would grow to failure. Because of the steep R curve caused by the fiber bridging, even if the W_f model accurately predicted the initiation of damage, it might not predict failure because the damage may grow stably long after initiation. For these reasons, it may be that a more complex fracture model will be able to explain the fracture results, and then be used to relate the viscoelastic matrix response to the effect of loading rate on strength. Another possibility is that the $90°$ strength response is not controlled by a fracture phenomenon, and therefore a different type of model should be used.

An alternative failure criterion to the fracture model is the dilatational strain energy density model. As shown in the analysis chapter, the results from assuming that a critical dilatational strain energy density controls failure would be identical, for a given geometry, to the predictions from the fracture model which assumed that failure is controlled by the initiation of crack growth. The new model might explain why the fracture model seemed to do a reasonable job of modeling the transverse strength, as seen in Figure 26, once the critical value was allowed to vary, yet did not model the DCB fracture tests well. The dilatational strain energy model would make the same predictions seen in Figure 26 if the

critical value of strain energy density were allowed to vary with time and temperature as the W_f parameter was in Figure 25. The dilatational strain energy model would not however imply a similar response from the fracture specimen. Since the DCB toughness values did not form a master curve as expected based on the fracture model, the strain energy model seems an attractive alternative. The dilatational strain energy model is presented here as an alternative explanation for the results, but the current results can in no way be seen as a proof that the energy criterion is correct.

If the failure criterion is accurate, the model still has the problem that the W_f model had, in that the critical value was found to change with time and temperature. For these constant ramp tests, the parameter changed in a well behaved manner, but to apply these results to other temperature-load histories would require a more thorough understanding of the cause of this change than can be determined from the current study.

Although it is disappointing that both the fracture model and the dilatational strain energy density model failed to explain the observed strength response in a way that can be applied to tests with other load-temperature histories, the fact that a master curve was created by the strength data indicates that temperature can be used to accelerate strength tests. The significant drop in strength with higher temperatures and slower loading rates also shows that it is important to account for time scale when using strength in structural designs. Without a model to explain the master curve results, the accelerated test methodology is not very useful. With the current results, the 90° strength at temperatures and loading rates not tested can be predicted, but to predict the strength after an arbitrary loading history would be impossible. Simply adding a hold during the constant load rate test would change the strength results in a way that could not be predicted using the current results without a more robust model to back up the experimental data. Changing temperature during a test would equally complicate the results so that creating an accelerated test for such a case would be difficult. Because strength testing is so expensive and time consuming, an accelerated test that does not allow the prediction of strength due to an arbitrary loading and temperature

history is probably not very useful. It is simply too expensive to try to test for the different loading and temperature permutations. The most significant result of this research is not the accelerated test methodology, but the hope that a more robust model may be possible and the proof that it is indeed needed.

CHAPTER VI

CONCLUDING REMARKS

The use of time-temperature superposition has been shown to apply to the transverse tensile strength of a thermoplastic composite material using the same shift factors as measured for compliance. This was demonstrated with transverse tension strength data for IM7/K3B at four temperatures from 300°F to 450°F and at five different loading rates that produced failure in the range from 0.5 sec to 24 hours. This accelerated test method applied well up to 400°F where a master curve could be formed from the experimental data. The master curve showed that a composite might loose 50% of its strength over 9 decades of time. Results at 450°F, however, did not fit on the master curve.

To explain why the same shifts rates might apply to both strength and compliance, a viscoelastic fracture model was investigated based on the hypothesis that transverse strength is controlled by the work of fracture for crack initiation from a critical flaw. The viscoelastic J integral theory and the elastic-viscoelastic correspondence principle were used to obtain an expression for the energy at the crack tip in terms of the viscoelastic compliance. It was hoped that the critical crack tip energy level for fracture would remain constant with time and temperature. The time-dependent nature of strength would therefore be controlled by the time-dependent compliance properties used as input to the model. The model was found to fit the strength data only if the critical energy parameter was allowed to vary as an exponential with loading rate.

To validate the fracture model, fracture tests using double cantilever beam specimens were conducted from 300°F to 400°F over the same time scales as for the strength tests. The delamination fracture toughness determined in these tests showed a significant change with loading rate, but less of a variation with temperature, and did not form a master curve. At the lower temperatures, the toughness decreased by 60% over the five decades of time tested. The material was found to have a large R-curve effect where the toughness increased

83

with crack growth. This phenomenon complicated the data reduction of the tests and was assumed to be due to fiber bridging, and therefore, only an artifact of the uniaxial test specimen. The fracture results could not be modeled with the fracture model, making the model's application to the transverse tensile strength test results questionable.

An alternative explanation for the strength results was offered by a dilatational strain energy density failure criterion. The use of a micromechanics model and a viscoelastic correspondence principle produced predictions of transverse strength that varied with time and temperature by the same amounts as predicted by the fracture model. This model however is a strength based model instead of a fracture model so it would not be expected to apply to the delamination fracture toughness results. With this model, the critical parameter still varied exponentially with loading rate. Because the critical parameter changes with loading rate, how it would change with other time and temperature histories is uncertain. This severely limits the use of both models in the development of accelerated test methodologies.

The significance of this research is therefore seen as providing the hope that a more versatile acceleration method for strength can be developed while also providing the proof that such a test is needed. The promise of an accelerated test method comes from the strength data forming a master curve. The need for an accelerated test is demonstrated by the significant decrease in both the strength data and the toughness data over the five decades of time tested.

REFERENCES

[1] Brunner, M. D. and A. Velicki. 1993. "Viability Trade Studies for High Speed Civil
     Transport," in *Fourth NASA/DoD Advanced Composites Technology Conference*,
     Vol. 1, pp. 881-906.

[2] Cregger, S. E., J. A. Pierre, P. G. Rimbos and L. Suju. 1993. "Materials, Structures,
     and Manufacturing Studies for the High Speed Civil Transport," in *Fourth
     NASA/DoD Advanced Composites Technology Conference*, Vol. 1, pp. 907-946.

[3] Case, S. W. and K. L. Reifsnider. 1997. "MRLIFE10 Simulation of Performance
     and Life Prediction for Composite Laminates," Blacksburg, VA: Virginia
     Polytechnic Institute and State University, August.

[4] Kim, H. J., D. M. Harmon, S. P. Wanthal and C. R. Saff. 1993. "Integrated
     Physical/Mechanical Analysis of Aged Polymer Matrix Composites," in *Fourth
     NASA/DoD Advanced Composites Technology Conference*, Vol. 1, pp. 1037-1052.

[5] Allix, O., P. Ladevéze and L. Perret, Eds. 1993. *Une nouvelle approche des
     composites par la mécanique de l'endommagement*, Cachan, France: l'ENS de
     Cachan.

[6] Schroedter, R. D., III and C. T. Herakovich. 1995. "Damage Evolution in IM7/K3B
     Carbon-Polyimide Composite," No. HTC-95-0C-A, Charlottesville, VA:
     University of Virginia, December.

[7] Talreja, R., Ed. 1994. *Damage Mechanics of Composite Materials*, Vol. 9, New
     York: Elsevier.

[8] Reifsnider, K. L., Ed. 1991. *Fatigue of Composite Materials*, Vol. 4, New York:
     Elsevier.

[9] Schapery, R. A. 1974. "Viscoelastic Behavior and Analysis of Composite
     Materials," Ch. 4 *of Mechanics of Composite Materials*, Vol. 2, Sendeckyj, Ed.
     New York: Academic Press, pp. 85-168.

[10] Dillard, D. A. 1990. "Viscoelastic Behavior of Laminated Composite Materials," Ch. 8 of *Fatigue of Composite Materials*, Vol. 4, *Composite Materials Series*. New York: Elsevier, pp. 339-384.

[11] Scott, D. W., J. S. Lai and A.-H. Zureick. 1995. "Creep Behavior of Fiber-Reinforced Polymeric Composites: A Review of the Technical Literature," *Journal of Reinforced Plastics and Composites*, 14:588-617.

[12] Rodriquez, P. I. 1993. "On the Design of Structural Components Using Materials with Time-Dependent Properties," NASA TM108428, October.

[13] Tuttle, M. E., A. Pasricha and A. F. Emery. 1995. "The Nonlinear Viscoelastic-Viscoplastic Behavior of IM7/5260 Composites Subjected to Cyclic Loading," *Journal of Composite Materials*, 29(15):2025-2046.

[14] Moore, R. H. and D. A. Dillard. 1990. "Time-Dependent Matrix Cracking in Cross-Ply Laminates," *Composites Science and Technology*, 39(1):1-12.

[15] Brinson, H. F. 1984. "Viscoelastic Behavior and Lifetime (Durability) Predictions," in *Mechanical Characterization of Load Bearing Fibre Composite Laminates*, A. H. Cardon and G. Verchery, Eds. New York: Elsevier, pp. 3-20.

[16] Martin, R. H., E. J. Siochi and T. S. Gates. 1992. "Isothermal Aging of IM7/8320 and IM7/5260," NASA TM 107666, August.

[17] Scola, D. A. and J. H. Vontell. 1988. "High Temperature Polyimides, Chemistry and Properties," *Polymer Composites*, 9(6):443-452.

[18] Cardon, A. H., C. C. Hiel, R. Brouwer, W. P. De Wilde, H. Sol, D. Van Hemelrijck and X. Xinran. 1988. "Time and Environmental Effects on the Long-term Behaviour of Structures Built Up from Polymeric Matrix Composites and Adhesive Joints," in *Engineering Applications of New Composites*. Wallingford: Omega Scientific, pp. 465-475.

[19] Hipp, R. C. and A. R. Mallow. 1993. "Accelerated Test Methodology Development for Polymer Composite Materials," in *Fourth NASA/DoD Advanced Composites Technology Conference*, Vol. 1, pp. 1017-1035.

[20] Struik, L. C. E. 1978. *Physical Aging in Amorphous Polymers and Other Materials*, New York: Elsevier.

[21] Feldman, M. 1996. "The Effects of Elevated Temperature on the Physical Aging of a High Temperature Thermoplastic Resin and Composite," Ph.D. dissertation in Engineering Mechanics. Norfolk, VA: Old Dominion University.

[22] Gates, T. S. and M. Feldman. 1994. "The Effects of Physical Aging at Elevated Temperatures on the Viscoelastic Creep of IM7/K3B," NASA TM 109114, June.

[23] Hastie, R. L., Jr. and D. H. Morris. 1993. "The Effects of Physical Aging on the Creep Response of a Thermoplastic Composite," in *High Temperature and Environmental Effects on Polymeric Composites, ASTM STP 1174*, C. E. Harris and T. S. Gates, Eds. Philadelphia: American Society for Testing and Materials, pp. 163-185.

[24] Castelli, M. G. 1994. "An Advanced Test Technique to Quantify Thermomechanical Fatigue Damage Accumulation in Composite Materials," *Journal of Composites Technology & Research*, 16(4):323-328.

[25] Roberts, G. D., B. P. H. Ho and J. F. Wallace. 1993. "Effects of Thermal and Mechanical Fatigue on the Flexural Strength of G40-600/PMR-15 Cross-Ply Laminates," NASA TM 106016, February.

[26] Pasricha, A., M. E. Tuttle and A. F. Emery. 1996. "Time-Dependent Response of IM7/5260 Composites Subjected to Cyclic Thermo-Mechanical Loading," *Composite Science and Technology*, 56:55-62.

[27] Haskins, J. F., J. R. Kerr and B. A. Stein. 1977. "Flight Simulation Testing of Advanced Composites for Supersonic Cruise Aircraft Applications," in *18th*

AIAA/ASME Structures, Structural Dynamics & Materials Conference, Vol. A, pp. 236-244.

[28] Whitney, J. M. and C. E. Browning. 1984. "Materials Characterization for Matrix Dominated Failure Modes," in *Effects of Defects in Composite Materials, ASTM STP 836.* Philadelphia: American Society for Testing and Materials, pp. 104-124.

[29] Asp, L. E., L. A. Berglund and R. Talreja. 1996. "Prediction of Matrix-Initiated Transverse Failure in Polymer Composites," *Composites Science and Technology*, 56:1089-1097.

[30] Asp, L. E. and L. A. Berglund. 1996. "A Criterion for Crack Initiation in Glassy Polymers Subjected to a Composite-Like Stress State," *Composite Science and Technology*, 56:1089-1097.

[31] Asp, L. E., L. A. Berglund and R. Talreja. 1996. "Effects of Fiber and Interphase on Matrix Initiated Transverse Failure in Polymer Composites," *Composite Science and Technology*, 56:657-665.

[32] Meurs, P. 1997. "Characterization of Microphenomenon in Transversely Loaded Composite Materials," Ph.D. dissertation in Polymer Chemistry and Technology. Eindhoven, The Netherlands: Eindhoven University of Technology.

[33] Ishai, O., R. M. Anderson and R. E. Lavengood. 1970. "Failure-Time Characteristics of Continuous Unidirectional Glass-Epoxy Composites in Flexure," *Journal of Materials*, 5(1):184-208.

[34] Bueche, F. 1957. "Tensile Strength of Plastics Below the Glass Temperature," *Journal of Applied Physics*, 28(7):784-787.

[35] Bueche, F. 1962. *Physical Properties of Polymers*, New York: Interscience.

[36] Govaert, L. E., R. J. M. Smit and T. Peijs. 1997. "Micromechanical Modelling of Time-Dependent Failure in Transversely Loaded Composites," in *Proceedings of the 10th International Conference on Deformation, Yield and Fracture of Polymers,* London: Institute of Materials, pp. 427-430.

[37] Ward, I. M. 1990. *Mechanical Properties of Solid Polymers*, second ed. Chichester, England: John Wiley and Sons.

[38] Berglund, L. A., J. Varna and J. Yuan. 1991. "Effect of Intralaminar Toughness on the Transverse Cracking Strain in Cross-ply Laminates," *Advanced Composite Materials*, 1(3):225-234.

[39] Frassine, R. and A. Pavan. 1995. "Viscoelastic Effects on the Interlaminar Fracture Behaviour of Thermoplastic Matrix Composites: I. Rate and Temperature Dependence in Unidirectional PEI/Carbon-Fibre Laminates," *Composites Science and Technology*, 54:193-200.

[40] You, H. and Y.-J. Yum. 1997. "Loading Rate Effect on Mode I Interlaminar Fracture of Carbon/Epoxy Composite," *Journal of Reinforced Plastics and Composites*, 16(6):537-549.

[41] Knauss, W. G. 1976. "Fracture of Solids Possessing Deformation Rate Sensitive Material Properties," in *The Mechanics of Fracture*, Vol. 19, F. Erdogan, Ed. New York: The American Society of Mechanical Engineers, pp. 69-103.

[42] Knauss, W. G. 1974. "On the Steady Propagation of a Crack in a Visco-Elastic Sheet: Experiments and Analysis," in *Deformation and Fracture of High Polymers*, Kausch, Hassel and Jaffe, Eds. New York: Plenum Press.

[43] Kim, K. S. and R. H. Van Stone. 1992. "Elevated Temperature Crack Growth," NASA CR-189191, December.

[44] Schapery, R. A. 1984. "Correspondence Principles and a Generalized J Integral for Large Deformation and Fracture Analysis of Viscoelastic Media," *International Journal of Fracture*, 25:195-223.

[45] Schapery, R. A. 1990. "On Some Path Independent Integrals and Their Use in Fracture of Nonlinear Viscoelastic Media," *International Journal of Fracture*, 42:189-207.

[46] Yoon, C. and D. H. Allen. 1999. "Damage Dependent Constitutive Behavior and Energy Release Rate for a Cohesive Zone in a Thermoviscoelastic Solid," *International Journal of Fracture*, 96(1):55-74.

[47] Ferry, J. D. 1970. *Viscoelastic Properties of Polymers*, New York: Wiley.

[48] Yeow, Y. T., D. H. Morris and H. F. Brinson. 1979. "Time-Temperature Behavior of a Unidirectional Graphite/Epoxy Composite," in *Composite Materials: Testing Design (fifth Conference), ASTM STP 674*, S. W. Tsai, Ed. Philadelphia: American Society for Testing and Materials, pp. 263-281.

[49] Williams, M. L., R. F. Landel and J. D. Ferry. 1955. "The Temperature Dependence of Relaxation Mechanisms in Amorphous Polymers and Other Glass-forming Liquids," *The Journal of the American Chemical Society*, 77(14):3701-3707.

[50] Lohr, J. J. 1965. "Yield Stress Master Curves for Various Polymers Below Their Glass Transition Temperatures," *Transactions of the Society of Rheology*, 9(1):65-81.

[51] Moehlenpah, A. E., O. Ishai and A. T. DiBenedetto. 1971. "The Effect of Time and Temperature on the Mechanical Behavior of Epoxy Composites," *Polymer Engineering and Science*, 11(2):129-138.

[52] Miyano, Y., M. Kanemitsu, T. Kunio and H. A. Kuhn. 1986. "Role of Matrix Resin on Fracture Strengths of Unidirectional CFRP," *Journal of Composite Materials*, 20:520-538.

[53] Mohri, M., Y. Miyano and M. Suzuki. 1991. "Time-Temperature Dependence on Flexural Strength of Pitch-Based Carbon Fiber Unidirectional CFRP Laminates," in *Composites: Design, Manufacture, and Application. Proceedings of the Eighth International Conference on Composite Materials*, S. W. Tsai and G. S. Springer, Eds. Covina, CA: SAMPE, pp. 33-B-1 to 9.

[54] Miyano, Y., M. Nakada, M. K. McMurray and R. Muki. 1997. "Prediction of Flexural Fatigue Strength of CFRP Composites Under Arbitrary Frequency, Stress Ratio and Temperature," *Journal of Composite Materials*, 31(6):619-638.

[55] Pride, R. A., B. A. Stein and F. W. Schmidt. 1968. "Mechanical Properties of Polyimide-Resin/Glass Fiber Laminates for Various Time, Temperature and Pressure Exposures," in *Proceedings of the 23rd Annual Technical Conference of the SPI Composites Institute, Section 17C,* Washington DC: SPI Composites Institute, pp. 1-8.

[56] Larson, F. R. and J. Miller. 1952. "A Time-Temperature Relationship for Rupture and Creep Stresses," *Transactions of ASME*, 74:765-771.

[57] Brinson, H. F., W. I. Griffith and D. H. Morris. 1981. "Creep Rupture of Polymer-matrix Composites," *Experimental Mechanics*, 21(9):329-336.

[58] Hercules Corp. 1989. "Hercules Prepreg Tape Materials Characterization Data Package," Magna, UT: Hercules Composite Products Group, February.

[59] Spiegelman, P. P., D. C. Aldrich and R. F. Waughtal. 1987. "Recent Developments in High Temperature Polyimide Systems," SAE Technical Paper Series, No. 871834, Warrendale, PA: Society of Automotive Engineers.

[60] Monagan, M. B., K. O. Geddes, K. M. Heal, G. Labahn and S. M. Vorkoetter. 1996. *Maple V Programming Guide*, New York: Waterloo Maple Inc.

[61] Alfrey, T. 1944. "Nonhomogeneous Stresses in Viscoelastic Media," *Quarterly of Applied Mathematics*, 2:113-119.

[62] ASTM. 1994. "Standard Test Method for Mode I Interlaminar Fracture Toughness of Unidirectional Fiber-Reinforced Polymer Matrix," No. D5528-94a, Philadelphia: American Society of Testing and Materials.

[63] Goetz, D. P. 1988. "Determination of the Mode I Delamination Fracture Toughness of Multidirectional Composite Laminates," Ph.D. dissertation in Mechanical Engineering. College Station, TX: Texas A&M University.

[64] Brown, W. F., Jr. and J. E. Strawley. 1966. *Plane Strain Crack Toughness Testing of High Strength Metallic Materials, ASTM STP 410*, Philadelphia: American Society of Testing and Materials.

[65] Kinloch, A. J. and S. Young. 1985. *Flow and Fracture of Polymers*, New York: Elsevier.

[66] de Charentenay, F. X., J. M. Harry, Y. J. Prel and M. L. Benzeggagh. 1984. "Characterizing the Effect of Delamination Defect by Mode I Delamination Test," in *The Effect of Defects in Composite Materials, ASTM STP 836*, D. J. Wilkins, Ed. Philadelphia: American Society for Testing and Materials, pp. 84-103.

[67] Russell, A. J. 1982. "Factors Affecting the Opening Mode Delamination of Graphite Epoxy Laminates," No. DREP 82-Q, Victoria, B. C.: Defense Research Establishment Pacific.

[68] Johnson, W. S. and P. D. Mangalgari. 1987. "Investigation of Fiber Bridging in Double Cantilever Beam Specimens," *Journal of Composite Technology and Research*, 9:10-13.

APPENDIX

Table 1. Transverse Tension Strength Data.

Specimen No.	Width	Thick.	Temp.	Rate	Shifted Rate	P_{max}	Strength	Comments
	in.	in.	°F	lb/sec	lb/sec	lb.	psi	
34-05	1.500	0.0438	300	0.0025	2.5E-03	226	3440	failure at tab
32-15	1.500	0.0441	300	0.0025	2.5E-03	267	4036	failure at tab
32-11	1.500	0.0437	300	0.0025	2.5E-03	270	4119	poor alignment
36-03	1.500	0.0442	300	0.05	5.0E-02	273	4118	
32-14	1.500	0.0445	300	0.05	5.0E-02	293	4390	failure at tab
32-17	1.500	0.0432	300	0.05	5.0E-02	313	4830	failure near tab
32-22	1.500	0.0434	300	1	1.0E+00	319	4900	failure at tab
32-12	1.500	0.0442	300	1	1.0E+00	332	5008	
32-04	1.500	0.0437	300	1	1.0E+00	350	5339	
33-13	1.500	0.0436	300	25	2.5E+01	329	5031	failure at tab
36-25	1.500	0.0441	300	25	2.5E+01	345	5215	
33-23	1.500	0.0444	300	25	2.5E+01	355	5330	failure at grip
34-17	1.500	0.0441	300	500	5.0E+02	383	5790	
35-10	1.500	0.0433	300	500	5.0E+02	394	6066	
32-30	1.500	0.0434	300	500	5.0E+02	401	6160	
35-05	1.500	0.0429	350	0.0025	9.6E-06	192	2984	failure at tab
35-05	1.500	0.0432	350	0.0025	9.6E-06	197	3040	failure at tab
34-09	1.515	0.0440	350	0.0025	9.6E-06	198	2975	
36-26	1.500	0.0448	350	0.05	1.9E-04	229	3408	
34-14	1.500	0.0434	350	0.05	1.9E-04	229	3518	
32-23	1.510	0.0430	350	0.05	1.9E-04	244	3753	
33-07	1.500	0.0437	350	1	3.9E-03	252	3844	failure at tab
35-09	1.500	0.0444	350	1	3.9E-03	269	4039	
32-18	1.509	0.0435	350	1	3.9E-03	292	4448	
34-28	1.507	0.0438	350	25	9.6E-02	294	4454	poor alignment
32-28	1.510	0.0442	350	25	9.6E-02	322	4825	
32-06	1.500	0.0431	350	25	9.6E-02	326	5043	
35-26	1.500	0.0435	350	500	1.9E+00	317	4858	
35-12	1.505	0.0442	350	500	1.9E+00	324	4871	
34-15	1.500	0.0441	350	500	1.9E+00	327	4943	
33-19	1.500	0.0446	400	0.0025	7.1E-08	174	2601	failure at grip
32-03	1.500	0.0438	400	0.0025	7.1E-08	176	2679	failure at grip
32-05	1.505	0.0430	400	0.0025	7.1E-08	182	2812	
34-30	1.508	0.0436	400	0.05	1.4E-06	186	2835	
35-19	1.500	0.0438	400	0.05	1.4E-06	193	2938	failure at tab
blank	1.500	0.0444	400	0.05	1.4E-06	240	3604	failure at tab
36-24	1.500	0.0435	400	1	2.8E-05	202	3096	failure at tab
33-12	1.513	0.0437	400	1	2.8E-05	220	3320	
34-23	1.500	0.0435	400	1	2.8E-05	224	3433	failure near tab
36-13	1.500	0.0445	400	25	7.1E-04	235	3521	

Table 1. Continued.

Specimen No.	Width	Thick.	Temp.	Rate	Shifted Rate	P_{max}	Strength	Comments
	in.	in.	°F	lb/sec	lb/sec	lb	psi	
35-07	1.508	0.044	400	25	7.1E-04	258	3888	
32-29	1.500	0.044	400	25	7.1E-04	281	4258	
35-14	1.500	0.0442	400	500	1.4E-02	255	3846	
36-28	1.500	0.0444	400	500	1.4E-02	269	4039	failure near tab
35-08	1.507	0.0433	400	500	1.4E-02	294	4506	
33-16	1.500	0.0432	450	0.0025	8.9E-10	56	864	
33-10	1.500	0.0432	450	0.0025	8.9E-10	61	941	
33-20	1.500	0.0443	450	0.0025	8.9E-10	65	978	
34-20	1.500	0.0445	450	0.05	1.8E-08	87	1303	
36-20	1.500	0.0441	450	0.05	1.8E-08	91	1376	
32-21	1.500	0.0431	450	0.05	1.8E-08	91	1408	
34-12	1.500	0.0435	450	1	3.6E-07	117	1793	
34-26	1.500	0.0438	450	1	3.6E-07	121	1842	
34-08	1.500	0.0435	450	1	3.6E-07	129	1977	
35-29	1.500	0.0441	450	25	8.9E-06	179	2706	
36-10	1.500	0.0437	450	25	8.9E-06	179	2731	
34-03	1.500	0.0435	450	25	8.9E-06	181	2774	
35-25	1.500	0.0439	450	500	1.8E-04	240	3645	
33-02	1.500	0.0437	450	500	1.8E-04	243	3707	
33-18	1.500	0.0436	450	500	1.8E-04	262	4006	
data filtered out due to low strength values								
32-24	1.500	0.0433	300	0.0025	2.50E-03	217	3341	failure at grip
32-16	1.500	0.0437	300	0.0025	2.50E-03	172	2624	failure at grip
33-21	1.500	0.0435	300	0.0025	2.50E-03	165	2529	failure at grip
35-22	1.500	0.0434	300	0.05	5.00E-02	250	3840	
35-02	1.500	0.0432	300	0.05	5.00E-02	224	3457	failure at tab
36-16	1.500	0.0444	300	0.05	5.00E-02	206	3093	failure at tab
36-11	1.500	0.0445	300	0.05	5.00E-02	187	2801	failure at tab
35-01	1.500	0.0432	300	1	1.00E+00	234	3611	
35-27	1.500	0.043	300	1	1.00E+00	234	3628	failure near tab
35-23	1.500	0.0444	300	1	1.00E+00	225	3378	failure at tab
36-09	1.500	0.0442	300	25	2.50E+01	310	4676	
32-01	1.500	0.0432	300	25	2.50E+01	267	4120	poor alignment
36-18	1.500	0.0441	300	25	2.50E+01	263	3976	
35-20	1.496	0.044	350	0.00025	9.60E-07	142	2150	failure at grip
35-24	1.500	0.0426	350	0.00025	9.60E-07	104	1628	failure at grip
33-29	1.514	0.0438	350	0.0025	9.60E-06	159	2402	failure at grip
35-16	1.500	0.0439	350	0.0025	9.60E-06	132	2005	failure at grip
33-10	1.516	0.0438	350	0.0025	9.60E-06	110	1657	failure at grip
33-15	1.505	0.0437	350	0.05	1.90E-04	148	2250	failure at grip
33-14	1.512	0.0433	350	0.05	1.90E-04	144	2199	failure at grip

Table 1. Concluded.

Specimen No.	Width	Thick.	Temp.	Rate	Shifted Rate	P_{max}	Strength	Comments
	in.	in.	°F	lb/sec	lb/sec	lb	psi	
34-24	1.500	0.0434	350	1	3.90E-03	201	3088	failure at tab
36-05	1.500	0.0444	350	25	9.60E-02	237	3559	failure at tab
35-28	1.500	0.0434	350	25	9.60E-02	222	3410	
34-27	1.500	0.0442	350	500	1.90E+00	294	4434	
33-28	1.500	0.0441	350	500	1.90E+00	270	4082	
32-08	1.500	0.0432	400	0.0025	7.10E-08	151	2336	failure at grip
33-09	1.500	0.043	400	0.05	1.40E-06	186	2884	failure at grip
34-16	1.500	0.0443	400	0.05	1.40E-06	137	2068	
36-19	1.500	0.0449	400	1	2.80E-05	198	2940	
35-03	1.500	0.0437	400	10	2.80E-04	234	3570	
34-13	1.513	0.0438	400	25	7.10E-04	234	3531	poor alignment
35-17	1.500	0.0439	400	25	7.10E-04	223	3386	failure at tab
33-01	1.500	0.0438	400	25	7.10E-04	94	1431	damaged edges
33-26	1.500	0.0438	400	500	1.40E-02	246	3744	
36-15	1.500	0.0438	400	500	1.40E-02	225	3425	

Table 2. DCB Test Data.

Specimen No.	Width	Thick.	Temp	Load Rate	Shifted Rate	Slope m	P_{NL}	P_{MAX}	G_{Ic} (NL)	W_f(NL)
	in.	in.	°F	lb/sec	lb/sec	lb/in	lb.	lb.	in-lb/in²	in-lb/in²
3-40	1.003	0.1341	300	0.0003	3.00E-04	157	15.9	25.9	1.56	1.58
1-25	1.003	1.3380	300	0.0003	3.00E-04	160	16.4	27.2	1.62	1.66
2-41	1.004	0.1317	300	0.0003	3.00E-04	172	17.9	27.4	1.87	1.92
3-43	1.002	0.1346	300	0.0003	3.00E-04	157	17.8	26.6	2.01	2.06
2-34	1.006	0.1265	300	0.0003	3.00E-04	131	17.5	26.9	2.31	2.37
3-27	1.003	0.1343	300	0.006	6.00E-03	175	18.3	27.3	1.91	1.93
2-26	1.006	0.1354	300	0.006	6.00E-03	159	19.9	28.8	2.41	2.43
1-37	1.004	0.1344	300	0.006	6.00E-03	163	20.4	27.0	2.56	2.59
3-44	1.002	0.1272	300	0.006	6.00E-03	143	19.9	28.6	2.77	2.80
2-21	1.004	0.1330	300	0.006	6.00E-03	153	25.0	29.9	4.05	4.10
3-31	1.002	0.1337	300	0.12	1.20E-01	161	17.4	29.3	1.83	1.85
1-29	1.004	0.1333	300	0.12	1.20E-01	170	20.0	30.1	2.37	2.38
1-40	1.003	0.1326	300	0.12	1.20E-01	166	22.9	30.0	3.15	3.17
3-20	1.004	0.1353	300	0.12	1.20E-01	159	22.6	30.6	3.16	3.18
2-14	1.006	0.1332	300	0.12	1.20E-01	167	23.8	30.6	3.40	3.42
3-30	1.003	0.1343	300	3	3.00E+00	160	25.4	32.1	3.93	3.94
2-4	1.007	0.1354	300	3	3.00E+00	172	26.7	33.6	4.12	4.13
1-38	1.004	0.1335	300	3	3.00E+00	159	26.0	33.0	4.15	4.16
2-10	1.006	0.1343	300	3	3.00E+00	155	26.6	34.2	4.39	4.40
2-8	1.006	0.1346	300	3	3.00E+00	177	28.9	32.8	4.70	4.75
2-1	1.007	0.1260	300	52.9	5.29E+01	133	27.9	34.0	5.68	5.74
3-11	1.003	0.1280	300	58.8	5.88E+01	147	30.8	34.4	6.45	6.45
2-16	1.007	0.1344	300	60.0	6.00E+01	156	29.6	31.5	5.47	5.47
2-7	1.007	0.1340	300	64.5	6.45E+01	161	29.5	32.7	5.36	5.36
2-43	1.005	0.1338	300	65.8	6.58E+01	163	32.8	35.7	6.70	6.71
1-20	1.001	0.1350	350	0.0003	1.16E-06	174	17.5	27.6	1.79	1.97
2-6	1.007	0.1339	350	0.0003	1.16E-06	145	17.6	26.7	2.13	2.35
2-13	1.007	0.1320	350	0.0003	1.16E-06	134	17.3	25.2	2.16	2.38
1-42	1.004	0.1343	350	0.0003	1.16E-06	172	19.8	28.5	2.36	2.62
1-41	1.004	0.1236	350	0.0003	1.16E-06	172	21.2	27.9	2.62	2.91
1-32	1.004	0.1345	350	0.006	2.31E-05	183	18.9	27.0	1.95	1.97
2-36	1.005	0.1346	350	0.006	2.31E-05	162	18.0	28.7	2.01	2.09
3-22	1.002	0.1280	350	0.006	2.31E-05	140	17.3	26.9	2.13	2.22
3-35	1.003	0.1327	350	0.006	2.31E-05	218	21.0	32.1	2.29	2.39
1-34	1.003	0.1318	350	0.006	2.31E-05	131	18.3	26.8	2.55	2.58
1-26	1.003	0.1346	350	0.12	4.62E-04	162	19.0	31.5	2.21	2.25
3-38	1.003	0.1334	350	0.12	4.62E-04	164	19.8	28.5	2.40	2.44
3-37	1.004	0.1333	350	0.12	4.62E-04	227	22.6	30.9	2.53	2.58
1-9	1.005	0.1346	350	0.12	4.62E-04	205	23.0	33.2	2.76	2.81
1-15	1.000	0.1346	350	0.12	4.62E-04	161	22.1	30.2	3.06	3.11

Table 2. Concluded.

Specimen No.	Width	Thickness	Temp	Load Rate	Shifted Rate	Slope m	P_{NL}	P_{MAX}	G_{Ic} (NL)	W_f (NL)
	in.	in.	°F	lb/sec	lb/sec	lb/in	lb.	lb.	in-lb/in²	in-lb/in²
1-6	1.003	0.1341	350	3	1.16E-02	165	22.7	30.0	3.08	3.12
3-21	1.002	0.1340	350	3	1.16E-02	206	24.8	32.7	3.21	3.23
3-36	1.003	0.1331	350	3	1.16E-02	164	23.2	32.7	3.26	3.28
1-31	1.003	0.1351	350	3	1.16E-02	162	26.1	32.4	4.16	4.19
2-44	1.006	0.1265	350	3	1.16E-02	146	25.5	31.6	4.43	4.46
1-23	1.003	0.1235	350	50.0	1.93E-01	125	27.0	30.8	5.75	5.77
3-33	1.002	0.1282	350	57.9	2.23E-01	145	29.5	32.3	5.96	5.98
2-9	1.007	0.1337	350	60.6	2.33E-01	151	31.4	33.9	6.47	6.49
1-3	1.004	0.1345	350	62.9	2.42E-01	154	28.5	30.9	5.12	5.17
2-39	1.006	0.1336	350	64.6	2.49E-01	161	29.5	32.5	5.38	5.44
1-2	1.003	0.1349	400	0.0003	8.50E-09	150	21.5	23.3	3.01	3.05
1-4	1.004	0.1343	400	0.0003	8.50E-09	153	21.7	23.6	3.07	4.61
1-13	1.004	0.1345	400	0.0003	8.50E-09	155	22.4	27.1	3.23	3.27
1-35	1.003	0.1318	400	0.0003	8.50E-09	151	22.5	25.7	3.37	5.08
2-4	1.004	0.1340	400	0.0003	8.50E-09	156	24.0	24.9	3.62	5.50
2-40	1.005	0.1337	400	0.006	1.70E-07	176	19.6	25.9	2.14	2.51
2-11	1.007	0.1280	400	0.006	1.70E-07	137	19.5	27.4	2.69	3.16
2-18	1.007	0.1336	400	0.006	1.70E-07	156	20.7	27.6	2.75	3.23
1-33	1.005	0.1397	400	0.006	1.70E-07	142	20.8	27.4	2.95	2.99
2-22	1.005	0.1268	400	0.006	1.70E-07	147	21.1	28.7	3.03	3.56
2-29	1.005	0.1337	400	0.12	3.40E-06	155	20.4	30.1	2.68	2.86
1-17	1.003	0.1344	400	0.12	3.40E-06	161	22.3	30.5	3.00	3.21
2-42	1.005	0.1335	400	0.12	3.40E-06	162	23.6	32.0	3.43	3.67
1-22	1.002	0.1259	400	0.12	3.40E-06	146	22.8	32.0	3.57	3.83
3-12	1.002	0.1288	400	0.12	3.40E-06	141	23.6	32.8	3.92	4.20
3-5	1.007	0.1340	400	3	8.50E-05	162	21.4	32.6	2.76	2.83
1-39	1.004	0.1333	400	3	8.50E-05	170	23.3	36.7	3.18	3.27
1-30	1.004	0.1342	400	3	8.50E-05	158	22.7	30.0	3.18	3.22
1-1	1.003	0.1345	400	3	8.50E-05	172	24.2	34.2	3.46	3.56
2-23	1.006	0.1256	400	3	8.50E-05	139	22.3	33.4	3.58	3.68
3-24	1.004	0.1316	400	59.6	1.69E-03	150	26.9	34.9	4.71	4.76
1-28	1.004	0.1336	400	60.8	1.72E-03	157	24.3	34.8	3.71	3.75
2-37	1.006	0.1345	400	61.3	1.74E-03	157	24.5	32.0	3.78	3.82
2-17	1.007	0.1338	400	61.7	1.75E-03	155	24.6	30.5	3.82	3.86
2-38	1.006	0.1339	400	63.9	1.81E-03	161	27.7	34.7	4.78	4.83

1. AGENCY USE ONLY *(Leave blank)*	2. REPORT DATE August 2002	3. REPORT TYPE AND DATES COVERED Technical Memorandum

4. TITLE AND SUBTITLE	5. FUNDING NUMBERS
Prediction of Long-Term Strength of Thermoplastic Composites Using Time-Temperature Superposition	721-21-30-05

6. AUTHOR(S)

James R. Reeder

7. PERFORMING ORGANIZATION NAME(S) AND ADDRESS(ES)	8. PERFORMING ORGANIZATION REPORT NUMBER
NASA Langley Research Center Hampton, VA 23681-2199	L-18220

9. SPONSORING/MONITORING AGENCY NAME(S) AND ADDRESS(ES)	10. SPONSORING/MONITORING AGENCY REPORT NUMBER
National Aeronautics and Space Administration Washington, DC 20546-0001	NASA/TM-2002-211781

11. SUPPLEMENTARY NOTES

12a. DISTRIBUTION/AVAILABILITY STATEMENT	12b. DISTRIBUTION CODE
Unclassified-Unlimited Subject Category 24 Distribution: Nonstandard Availability: NASA CASI (301) 621-0390	

13. ABSTRACT *(Maximum 200 words)*

Accelerated tests for composite failure were investigated. Constant ramp transverse strength tests on thermoplastic composite specimens were conducted at four temperatures from 300°F to 450°F and five duration times from 0.5 sec to 24 hrs. Up to 400°F, the time-temperature-superposition method produces a master curve allowing strength at longer times to be estimated from strength tests conducted over shorter times but at higher temperatures. The shift factors derived from compliance tests applied well to the strength data. To explain why strength behaved similar to compliance, a viscoelastic fracture model was investigated based on the hypothesis that the work of fracture for crack initiation at some critical flaw remains constant with time and temperature. The model, which used compliance as input, was found to fit the strength data only if the critical fracture energy was allowed to vary with stress rate. Fracture tests using double cantilever beam specimens were conducted from 300°F to 450°F over time scales similar to the strength study. The toughness data showed a significant change with loading rate, less variation with temperature, did not form a master curve, and could not be correlated with the fracture model. Since the fracture model did not fit the fracture data, an alternative explanation based on the dilatational strain energy density was proposed. However the usefulness of this model is severely limited because it relies on a critical parameter which varies with loading rate.

14. SUBJECT TERMS	15. NUMBER OF PAGES
Thermoplastic resin; Resin matrix composite; Accelerated testing; Toughness; Viscoelasticity; Tension test; Fracture strength; Time temperature superposition	111
	16. PRICE CODE

17. SECURITY CLASSIFICATION OF REPORT	18. SECURITY CLASSIFICATION OF THIS PAGE	19. SECURITY CLASSIFICATION OF ABSTRACT	20. LIMITATION OF ABSTRACT
Unclassified	Unclassified	Unclassified	UL